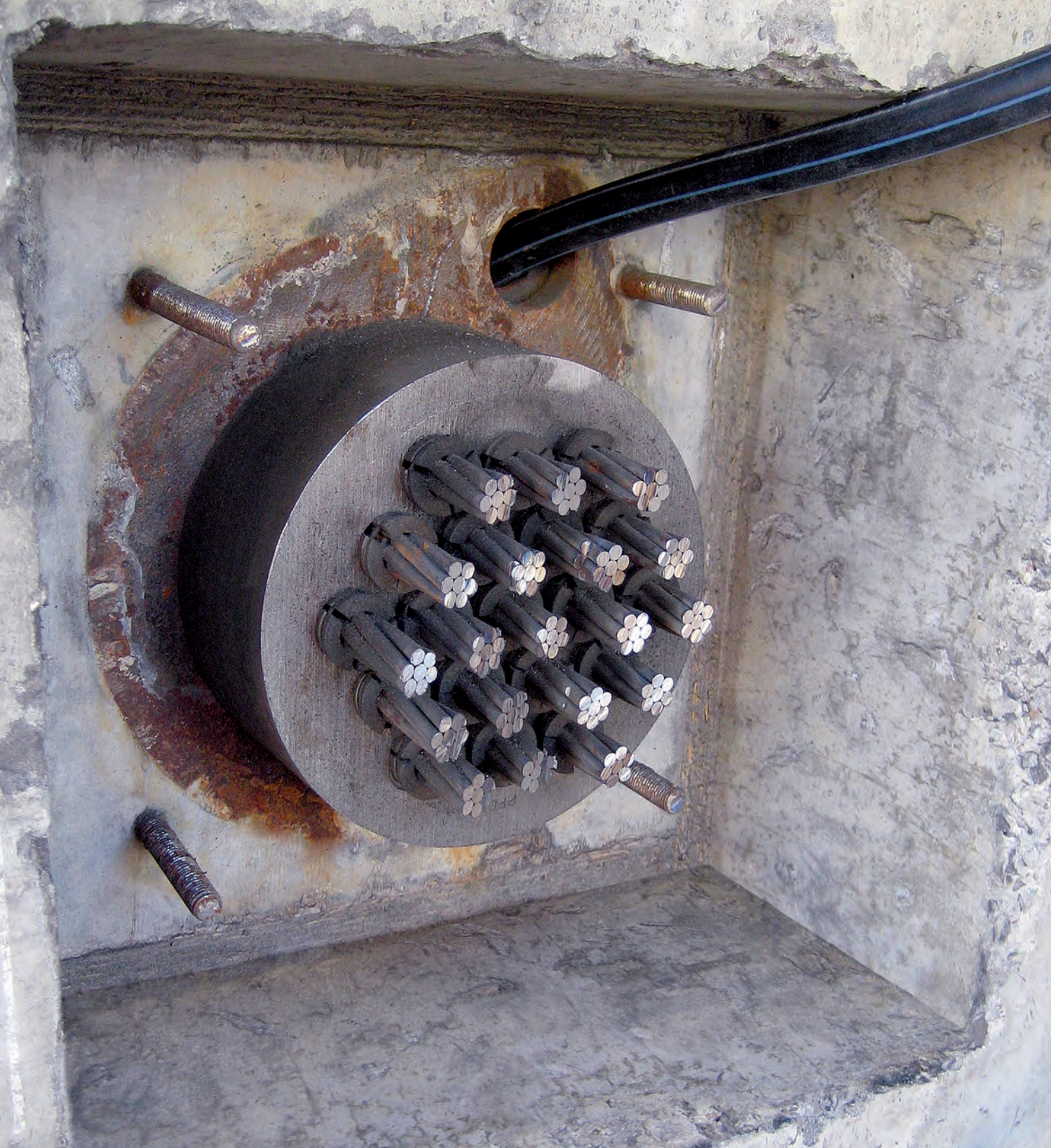


STRUCTURE AND ENVIRONMENT

ARCHITECTURE, CIVIL ENGINEERING, ENVIRONMENTAL ENGINEERING AND ENERGY

No. 1/2011 vol. 3 PL ISSN 2081-1500 www.sae.tu.kielce.pl KIELCE UNIVERSITY OF TECHNOLOGY



Contents

structure

ANDRZEJ S. NOWAK, ANNA M. RAKOCZY

DIAGNOSTIC PROCEDURES FOR ASSESSMENT OF STRUCTURES	5
--	---

GRZEGORZ MAZUREK

THE ASSESSMENT OF THE RESILIENT MODULUS OF ELASTICITY OF ASPHALT CONCRETE WITH LOW-VISCOSITY MODIFIER	16
--	----

ZDZISŁAWA OWSIAK, JUSTYNA ZAPAŁA

REVIEW OF THE LABORATORY METHODS APPLIED TO ASSESS THE REACTIVITY OF ALKALINE SILICEOUS AGGREGATES IN CONCRETE	21
---	----

environment

LIDIA DĄBEK, EWA OZIMINA, ANNA PICHETA-OŁĘŚ

ASSESSING THE EFFECT OF IRON IONS ADSORBED ON ACTIVATED CARBON AND THE EFFICIENCY OF DECOMPOSITION OF ORGANIC IMPURITIES USING SELECTED OXIDIZING AGENTS	29
---	----

EDYTA GROBELSKA

THE IMPACT OF MOISTURE AND CYCLIC FREEZING ON THE NON-FREEZING WATER OF MONO-IONIC BENTONITES	36
---	----

ŁUKASZ J. ORMAN

MEASUREMENTS OF BOILING HEAT TRANSFER ON A SINGLE FIN	47
---	----

HOW TO PREPARE THE MANUSCRIPT	53
-------------------------------------	----

THE REVIEW PROCESS	54
--------------------------	----

EDITORIAL BOARD

Main Editor Jerzy Z. Piotrowski

Editor Ludwik Śliwa

Secretary of the Editorial Board Radosław Zaborek

Sectional Editor STRUCTURE Zdzisława Owsiak

Sectional Editor ENVIRONMENT Lidia Dąbek

SCIENTIFIC BOARD

Chairmanship Tomasz Kozłowski

STRUCTURE

Tomasz Arciszewski (USA), Lesław Brunarski, Go Iwahana (Japan), Marek Iwański, Zbigniew Kowal, Jozef Melcer (Slovakia), Michał V. Nemchinov (Russia), Victor Proskuriakow, Zbigniew Rusin, Bohdan Rymaszewski, Wacław Seruga, Małgorzata Wilczkiewicz (USA)

ENVIRONMENT

Satoshi Akagawa (Japan), Elżbieta Bezak-Mazur, Dorota Chwieduk, Graham Herbertson (Scotland), Andrzej Kapłon, Andrzej Kuliczkowski, Janusz Łomotowski, Paweł Purgał, Leszek Radziszewski, Anatol Stroy (Ukraine), Maria Żygadło

www.sae.tu.kielce.pl

sae@tu.kielce.pl

The quarterly printed issues of Structure and Environment are their original versions

The Journal published by the Kielce University of Technology
Faculty of Civil and Environmental Engineering

PL ISSN 2081-1500

© Copyright by Wydawnictwo Politechniki Świętokrzyskiej, 2011

25-314 Kielce, al. Tysiąclecia Państwa Polskiego 7

tel. 41 34 24 581

www.tu.kielce.pl/organizacja/wydawnictwo



Kielce University of Technology

2011



structure
structure

ANDRZEJ S. NOWAK¹

ANNA M. RAKOCZY²

University of Nebraska,
Department of Civil Engineering,
Lincoln, NB, U.S.A.,

¹ e-mail: anowak2@unl.edu

² e-mail: arakoczy1@gmail.com

DIAGNOSTIC PROCEDURES FOR ASSESSMENT OF STRUCTURES

Abstract

The evaluation and verification of the actual loads, load carrying capacity and prediction of the remaining life are often required for existing structures. The objective of the paper is to present some of diagnostic techniques and examples of their practical applications. Diagnostic equipment such as strain measurement devices, deflection measurement equipment, optical and laser devices, accelerometers, tiltmeters, acoustic emission and crack control equipment as well as diagnostic procedures have been described.

Keywords: assessment of structures, diagnostic procedures

1. Introduction

Existing structures often require evaluation and verification of the actual loads and load carrying capacity as well as prediction of the remaining life. There are questions about the distribution of load on structural components, degree of deterioration and degradation of members and materials, assessment of deformations and displacements, occurrence and width of cracks, accumulation of fatigue load cycles, and so on. The analytical procedures are as accurate as the input data, i.e. assumptions about the boundary conditions, load and load distribution parameters, material behavior, redundancy and load sharing, contribution of nonstructural members, loss of section due to corrosion and other factors. It is a common practice to make conservative assumptions to account for uncertainties in quantification of these parameters in the analysis. However, the consequences of structural evaluation can call for an expensive repair, rehabilitation or replacement. Therefore, there is often a need for either a more detailed analysis and/or experimental verification of analytical assumptions using diagnostic procedures. Field tests confirm that the actual behavior of structures and its components is often very different than what is analytically predicted. For example, Bakht and Jaeger (1990) observed that the

actual load capacity of bridges is considerably higher than what is predicted by analytical methods. In certain cases, this extra safety reserve in the load capacity can be used to prove that the bridge is adequate and thus to avoid or delay expensive repair or replacement. On the other hand, although diagnostic tests are useful tools in structural evaluation, they cannot ensure that the part subjected to testing will not fail or malfunction. That is because every non-destructive test (NDT) has limitations and evaluation techniques should not be applied on a routine basis because of the difficulty of using the equipment and in the interpretation of the results due to lack of standardization (Hellier 2001; Abudayyeh et al. 2004).

The objective of this paper is to present some of diagnostic techniques and examples of practical applications.

2. Needs for diagnostic techniques

Diagnostic techniques are mostly used for verification of analytical models and the selection of equipment and methodology depends on the actual needs. The major questions relate to the loads and load carrying capacity. The needs can concern short-term or long-term parameters. Knowledge of the actual loads and load effects may require surveys and on-site measurements, for example:

- Natural loads such as wind, snow, ice, earthquake, temperature are recorded and the accumulated database can be used in prediction of structural load and load combinations. The required information includes magnitude and frequency of occurrence. Very important is simultaneous occurrence of loads and correlation between them. For each time-varying load, the statistical parameters include magnitude, return period, duration and coefficient of correlation with other loads.
- Live load in buildings. There is a need for recording the extreme load effects in various types, depending on function (apartments, offices, hotels, hospitals).
- Truck loads on highway bridges. The available techniques include weigh-in-motion (WIM) measurements with the objective to record all moving vehicles, with axle loads and spacing, lane position, speed, multiple presence with other vehicles.
- Fatigue load spectra. The measurements are focused on recording the strains in critical (fatigue-prone) components or connections, caused by load cycles, e.g. moving crane or vehicles.
- Dynamic loads. In structures designed for static and dynamic load components, there can be a need for verification of the extreme total load effect.
- Load distribution factors. This is verification of the structural analysis methods, to determine how is the load distributed on the load sharing members.
- Construction loads. Instrumentation can help monitor progressive changes in the loads and displacements/deformations during construction.
- Displacements and deformations. Structural performance can be unacceptable due to excessive deflection and/or vibration, or horizontal sway.
- Strain and stress. Load effect can be measured in terms on moments and shears, but the local effects are strains and stresses.
- Cracking in concrete. Brittle materials such as concrete can crack when in tension. The presence of crack can be unacceptable for various reasons (aesthetics, limited functionality, gradual deterioration). For example, in prestressed concrete beams exposed to the elements, multiple opening of cracks can lead to corrosion of strands.
- Fatigue cracks in steel. Occurrence and propagation of cracks can lead to collapse. Therefore, it is important to know when a crack initiated and if it keeps growing.

- Minimum load carrying capacity. Some structures are difficult to model analytically (e.g. complex geometry, unknown material properties, partially damaged, deteriorated, repaired) and there is a need to verify if they are adequate for normal use or operation.

3. Diagnostics equipment

3.1. Strain measurement devices

The strain transducer, shown in Figure 1, is one of the most important tools for the measurement of micro-displacements. They are used for the measurement of strain caused by an external influence or an internal effect such as forces, pressures, moments, heat, structural changes of the material, and the like. A strain transducer is a sensor whose resistance varies with applied force. It converts force, pressure, tension, weight, etc., into a change in electrical resistance which can then be measured. When it is stretched by applied force its resistance increases. Strain transducer should be installed in the same direction as the strain.

Experimental stress analysis uses the strain values measured on the surface of a specimen or structural part to state the stress in the material and also to predict its safety and endurance. Strain transducers are used to record the induced strains as a most direct approach to quantifying stress in a structural member. The transducer generally contains a pressure sensitive diaphragm with strain gages bonded to it.



Fig. 1. Reusable strain transducer mounted to the lower flange of a beam

When a load is applied to the surface, the resulting change in surface length is communicated to the resistor and the corresponding strain is measured in terms of the electrical resistance of the foil wire, which varies linearly with strain. The foil diaphragm and the adhesive bonding agent must work together in transmitting the strain, while the adhesive must also serve as an electrical insulator between the foil grid

and the surface. When selecting a strain transducer, one must consider not only the strain characteristics of the sensor, but also its stability and temperature sensitivity. Unfortunately, the most desirable strain gage materials are also sensitive to temperature variations and tend to change resistance as they age. For tests of short duration, this may not be a serious concern, but for continuous industrial measurement, one must include temperature and drift compensation.

In the past, strain transducer required a careful surface preparation and soldering to install. Now, most field strain gage installations can be replaced with a highly accurate new type strain transducer. These units are rugged and can be installed in any weather. Since they are pre-wired and easy to mount, they drastically reduce the field installation time.

The strain gages can be disposable or reusable. A new generation of these devices is wireless. It is important to note that strain measuring equipment requires power supply which is usually not available on the bridge. Then, power has to be provided by a generator or battery.

3.2. Deflection measurement equipment

The linear variable differential transformer (LVDT) is a type of electrical transformer used for measuring linear displacement. The transformer has three solenoid coils placed end-to-end around a tube. The center coil is the primary, and the two outer coils are the secondary. A cylindrical ferromagnetic core, attached to the object whose position is to be measured, slides along the axis of the tube. An alternating current is driven through the primary, causing a voltage to be induced in each secondary proportional to its mutual inductance with the primary. The frequency is usually in the range 1 to 10 kHz.

As the core moves, these mutual inductances change, causing the voltages induced in the secondary to change. The coils are connected in reverse series, so that the output voltage is the difference (hence "differential") between the two secondary voltages. When the core is in its central position, equidistant between the two secondary, equal but opposite voltages are induced in these two coils, so the output voltage is zero.

When the core is displaced in one direction, the voltage in one coil increases as the other decreases, cause the output voltage to increase from zero to a maximum. This voltage is in phase with the primary voltage. When the core moves in the other direction, the output voltage also increases from zero to a maximum, but its phase is opposite to that

of the primary. The magnitude of the output voltage is proportional to the distance moved by the core (up to its limit of travel), which is why the device is described as "linear". The phase of the voltage indicates the direction of the displacement.

Because the sliding core does not touch the inside of the tube, it can move without friction, making the LVDT a highly reliable device. The absence of any sliding or rotating contacts allows the LVDT to be completely sealed against the environment.

LVDTs are commonly used for measuring deflection in jointed reinforced concrete pavements, deflection of the deck under testing load and fatigue load.



Fig. 2. The linear variable differential transformer (LVDT)

3.3. Optical and laser devices

In the past decade, developing new nondestructive methods for bridge diagnosis has attracted serious attention. These techniques are used for bridge management to help enhance the cost-effectiveness of diagnosing bridges.

High-resolution images can be used to global diagnosis as a relatively new approach. These images can be provided using a couple current devices (CCD) or CCD camera. A typical camera has a sensor to receive light signals to be processed to form digital images. High-resolution images devices have many advantages in term of global diagnosis. One of them is no sensors required to attach to the bridge which significantly reduce a cost. Moreover, a large number of points can be covered for which measurement data are to be obtained. The large number of pixels offer unprecedented amount of spatially intensive data for effective diagnosis.

CCD image data can be effectively used for diagnosing structural stiffness loss. Laboratory experiments show that this method can detect structural damage as small as a 3 percent stiffness reduction.

High-resolution monitoring system can be used for bridges and also for buildings. This is very good solution for monitoring structural movement over the long-term such as: motion of bridge piers or building walls, the status of cracks in concrete and masonry, and strain levels induced during construction.

An additional contemporary method of NDT is Impact – Echo. This method base on an acoustic signal sends into the test specimen and record reflection from internal flaws, material layers or other interface. By analysis the reflected signal, conclusions about the depth of the reflecting surface can be show on graph. Impact – Echo method is commonly used in tunnel construction to check the required limiting thicknesses.

Total station is modern solution for measurement of deflection with accuracy up to 0.2 millimeters. This monitoring system is easier to set up and use, reducing labor and time requirements. The total station obtained three-dimensional coordinates of every target by measuring a horizontal angle, vertical angle, and distance between points. It automatically recorded the coordinates with a point number, point description, date, time, and atmospheric conditions [Merkle and Myers].

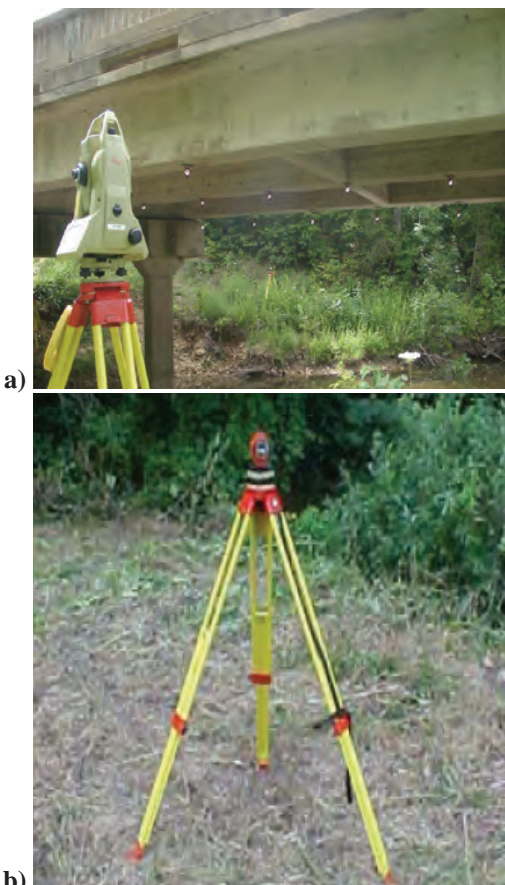


Fig. 3. Total station set up for load testing (a) and reference point (b)



Fig. 4. Target (prism) on a structural component

3.4. Accelerometers

An accelerometer is a device that measures the vibration, or acceleration of motion of a structure. The force caused by vibration or a change in motion (acceleration) causes the mass to “squeeze” the piezoelectric material which produces an electrical charge that is proportional to the force exerted upon it. Since the charge is proportional to the force, and the mass is a constant, then the charge is also proportional to the acceleration.

There are two types of piezoelectric accelerometers (vibration sensors). The first type is a “high impedance” charge output accelerometer. In this type of accelerometer the piezoelectric crystal produces an electrical charge which is connected directly to the measurement instruments. The charge output requires special accommodations and instrumentation most commonly found in research facilities. This type of accelerometer is also used in high temperature applications ($> 120^{\circ}\text{C}$) where low impedance models can not be used.

The second type of accelerometer is a low impedance output accelerometer. A low impedance accelerometer has a charge accelerometer as its front end but has a tiny built-in micro-circuit and FET transistor that converts that charge into a low impedance voltage that can easily interface with standard instrumentation. This

type of accelerometer is commonly used in industry. An accelerometer power supply like the ACC-PS1, provides the proper power to the microcircuit 18 to 24 V \pm 2 mA constant current and removes the DC bias level, they typically produces a zero based output signal up to +/- 5V depending upon the mV/g rating of the accelerometer. All OMEGA(R) accelerometers are this low impedance type.

3.5. Tiltmeters

A tiltmeter is an instrument designed to measure very small changes from horizontal level (angle of rotation). The most frequently it used for monitoring the response of structures to various influences such as loading and foundation settlement. Typical applications for tiltmeters include:

- Monitoring stabilization measures, such as pressure grouting and underpinning.
- Monitoring structures for the effects of tunneling and excavating.
- Monitoring the deflection and deformation of retaining walls.
- Monitoring convergence and other movements in tunnels.
- Providing early warning of threatening deformations, allowing time for corrective action to be taken.

The very first tiltmeter was a long-length stationary pendulum. These were used in the very first large concrete dams, and are still in use today, improved with newer technology such as laser reflectors. The modern electronic tiltmeter uses a simple bubble level principle, as used in the common carpenter level. An arrangement of electrodes senses the exact position of the bubble in the electrolytic solution, to a high degree of precision. Any small changes in the level are recorded using a standard cataloger. This arrangement is quite insensitive to temperature, and can be fully compensated, using built-in thermal electronics. Tiltmeters have also been extensively applied in the area of monitoring volcano and volcanic eruption prediction.

3.6. Acoustic emission

Acoustic Emission (AE) refers to the generation of transient elastic waves produced by a sudden redistribution of stress in a material or a small surface displacement. When a structure is subjected to an external stimulus (change in pressure, load, or temperature), localized sources trigger the release of energy, in the form of stress waves, which propagate to

the surface and are recorded by sensors. Earthquakes and rock bursts to the initiation and growth of cracks, slip and dislocation movements, melting, twinning, and phase transformations in metals are natural sources of AE. In composites, matrix cracking and fiber breakage and debonding contribute to acoustic emissions. AE's have also been measured and recorded in polymers, wood, and concrete, among other materials.

Detection and analysis of AE signals can supply valuable information regarding the origin and importance of a discontinuity in a material. Because of the versatility of Acoustic Emission Testing (AET), it has industrial applications in nondestructive testing and is used extensively as a research tool.

The application of AE to non-destructive testing of materials in the ultrasonic regime, typically takes place between 100 kHz and 1 MHz. Unlike conventional ultrasonic testing, AE tools are designed for monitoring acoustic emissions produced within the material during failure, rather than actively transmitting waves then collecting them after they have traveled through the material [Blitz and Simpson 1991]. Part failure can be documented during unattended monitoring. The monitoring of the level of AE activity during multiple load cycles forms the basis for many AE safety inspection methods that allow the parts undergoing inspection to remain in service.

The technique is used, for example, to study the formation of cracks during the welding process, as opposed to locating them after the weld has been formed with the more familiar ultrasonic testing technique [Blitz and Simpson 1991]. In a material under active stress, such as some components of an airplane during flight, transducers mounted in an area can detect the formation of a crack at the moment it begins propagating [Blitz and Simpson 1991]. A group of transducers can be used to record signals then locate the precise area of their origin by measuring the time for the sound to reach different transducers [Blitz and Simpson 1991]. The technique is also valuable for detecting cracks forming in pipelines transporting liquids under high pressures [Blitz and Simpson 1991].

3.7. Crack control equipment

The most frequently applied method for examining cracks uses a transducer on either side of a crack opening and the wave speed of the facial material replaces that of the interior wave speed according to ASTM C 1383 regulations [ASTM 1998]. However, after generating a stress wave, the front of a P wave must arrive first. Because the first transducer, A, is

closer to the wave source, S, the first transducer, A, may sense that P, S, and R waves are mixed, whereas the second transducer, B, located farther from S has an energy loss problem and cannot effectively measure the arriving waves. What is most significant is that almost all bridges have been given a surface finish, and consequently it is very hard to obtain the correct surface P wave speed for a structure whose surface has been weathered or has many cracks. Hence, using the wave speed as a replacement for speed of the interior material is likely inappropriate. Additionally, the cracks are typically within the area of tensile steels. Thus in practical applications, the ASTM methods are quite limited [Ming-Cheng Chen et al 2007].

Fatigue crack detection may be enhanced for visual examination by the unaided eye by using liquids to penetrate fatigue cracks. One method (liquid penetrate testing) involves using dyes, fluorescent or non-fluorescing, in fluids for non-magnetic materials, usually metals. Another commonly used method for magnetic materials involves using a liquid suspension of fine iron particles applied to a part while it is in an externally applied magnetic field (magnetic-particle testing).

4. Diagnostic procedures

4.1. Weigh-in-motion truck measurement

Weigh-in-motion (WIM) devices are designed to capture and record truck axle weights and gross vehicle weights as they drive over a sensor. Unlike older static weigh stations, current WIM systems do not require the subject trucks to stop making them much more efficient. Gross vehicle and axle weight monitoring is useful in an array of applications including: Pavement design, monitoring, and research; Bridge design, monitoring, and research; Size and weight enforcement; Legislation and regulation; Administration and planning.

The most widely accepted and utilized WIM contemporary devices in North America are: piezoelectric sensor, bending plate and single load cell.

Piezoelectric Sensors are the most common WIM device. The sensor is embedded in the pavement and produces a charge that is equivalent to the deformation induced by the tire loads on the pavement's surface. It is common to install two inductive loops and two piezoelectric sensors in each monitored lane. A properly installed and calibrated Piezoelectric WIM system can provide gross vehicle weights that are within 15% of the actual vehicle weight for 95% of the measured trucks.

The bending scale consists of two steel platforms that

are 0.6 x 2 m (2 ft. x 6 ft.), adjacently placed to cover a 3.65 m (12 ft.) lane. The plates are instrumented with strain gages, which measures tire load induced plate strains. The measured strains are then analyzed to determine the tire load. A properly installed and calibrated bending plate WIM system can provide gross vehicle weights that are within 10% of the actual vehicle weight for 95% of the measured trucks.

Single Load Cell device consists of two 3 x 3 m (6 ft. x 6 ft.) platforms placed adjacently to cover the 3.65 m (12 ft.) monitored lane. The scale mechanism incorporates patented load transfer torque tubes which effectively transfer all loading on the weighing surface to the load cell, which is mounted centrally in the scale. The system consists of two (2) steel frames (per lane) which are installed into existing or new asphalt or concrete pavement, and weigh pads which are bolted to the installation frame.

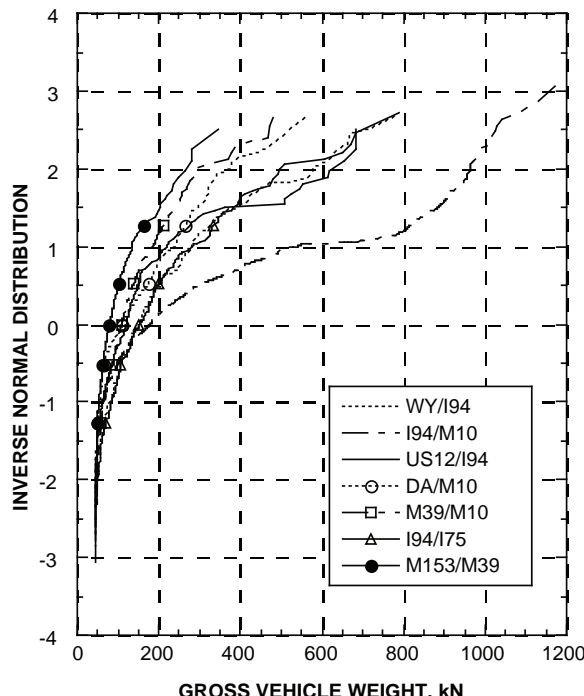


Fig. 5. CDF's of gross vehicle weight for different bridges

4.2. Verification of load distribution

Although modern computer techniques can provide detailed information about the load distribution in a bridge, the American Association of State Highway and Transportation Officials [AASHTO1998] Bridge Design Specifications provide a simple method for determining live load distribution, such that the bridge can be designed and analyzed as a series of beams, rather than a more complex three-dimensional structure. This makes routine design easy and provides

a simple and quick way to evaluate a bridge.

Field testing is an increasingly important topic in an effort to deal with the deteriorating infrastructure. There is a need for accurate inexpensive methods for diagnostics, verification of load distribution, and determination of the actual load-carrying capacity. A considerable number of bridges in Michigan were constructed in the 1950s and 1960s [Eom and Nowak 2001]. Many of them show signs of deterioration. In particular, there is severe corrosion on many steel and concrete structures. By analytical methods, some of these bridges are not adequate to carry the normal highway traffic. However, the actual load-carrying capacity is often much higher than what can be determined by analysis [Bakht and Jaeger 1990], due to more favorable load sharing, effect of nonstructural components (parapets, railing, and sidewalks), and other difficult to quantify factors. Field testing can reveal the hidden strength reserve and thus verify the adequacy of the bridge.

Previous research was presented by Kim and Nowak (1997) and Nowak et al. (1999, 2000). About 20 structures were selected as representative for the bridge inventory in the state of Michigan. For each structure, field tests and analysis were performed. The girders were instrumented, and strains and stresses were measured due to heavy trucks (up to 761 kN). GDFs were then calculated for one truck (one lane loaded) and two trucks side-by-side (two lanes loaded). The GDFs were also determined by the advanced structural analysis, based on the finite-element method (FEM). The currently available computer procedures allow for a very high degree of mathematical accuracy. However, the limitation, even for the latest generation of FEM programs, is the accuracy of input data, in particular, material properties and boundary conditions. The actual support conditions are difficult to represent analytically. Hinge-roller supports can be partially fixed (frozen) due to corrosion, accumulation of debris, and presence of a heavy diaphragm over the support. Nonstructural components such as sidewalks, curbs, and parapets contribute to the overall stiffness, and it is difficult to estimate this contribution analytically.

Loading uses in field test is chosen based on WIM data. For example, in Michigan, the maximum mid-span moment in medium span bridges is caused by 11-axle trucks, with gross vehicle weight (GVW) up to 730 kN depending the axle configuration [Eom and Nowak 2001]. This is almost twice the allowable legal load in other states. Most states allow a maximum GVW of 356 kN only with up to 5 axles per vehicle.

The vehicles used in the analysis in Michigan were fully loaded, three-unit, 11-axle trucks. A typical side-view of a truck used in the tests is shown in Figure 7. Analysis was performed under side-by-side truck loading condition.

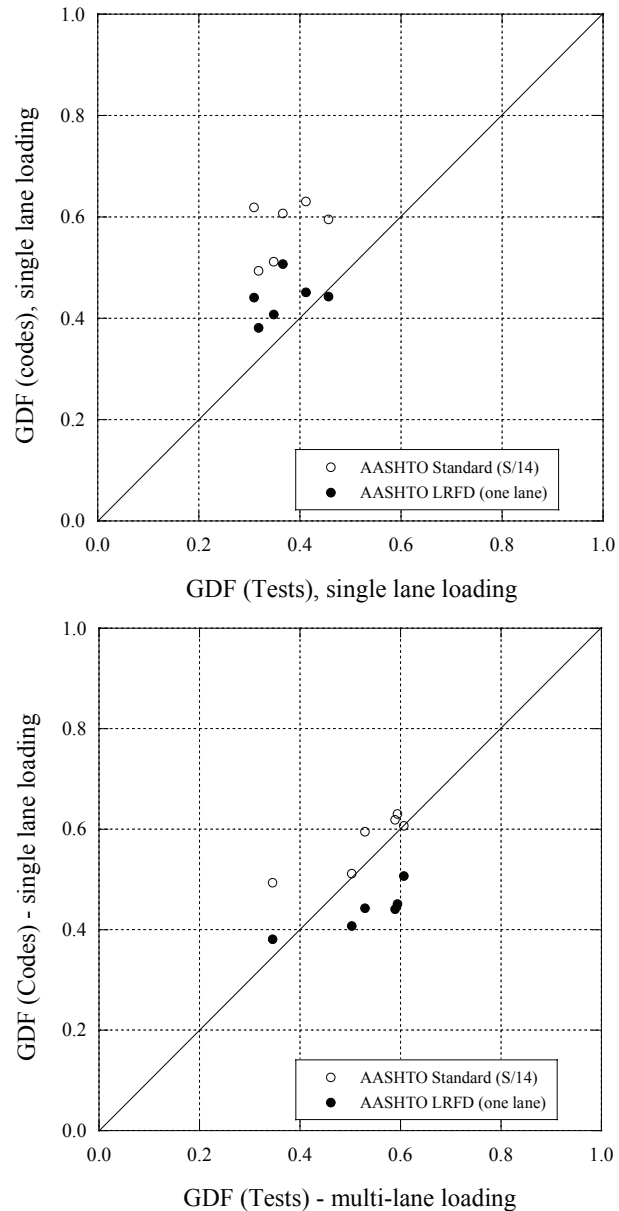


Fig. 6. Comparison of code specified vs. measured GDF's



Fig. 7. Truck used in diagnostic test

4.3. Verification of dynamic load

The dynamic load is time variant and random in nature and it depends on the vehicle type, vehicle weight, axle configuration, bridge span length, road roughness, and transverse position of a truck on the bridge. The dynamic load is usually considered as an equivalent static live load and is expressed in terms of dynamic load factor (DLF) [Nassif and Nowak 1995]. DLF is taken as a ratio of dynamic and static responses. In the AASHTO Standard (2002), dynamic load factors DLF are specified as a function of span length only (maximum 30 percent). In the AASHTO LRFD (2007), the dynamic load factor is equal to 0.33 of the truck effect, with no dynamic load applied to the uniform loading.

Field measurements are performed to determine the actual truck load effects and to verify the available analytical models [Nassif and Nowak 1995]. Measurements are taken using a system with strain transducers. For each truck passage, the dynamic response is monitored by recording strain data. The field measurements confirmed the results of analytical studies. The strain/stress due to dynamic load is nearly constant and is not dependant on static strain/stress. Therefore, the dynamic load factor is reduced for heavier trucks.

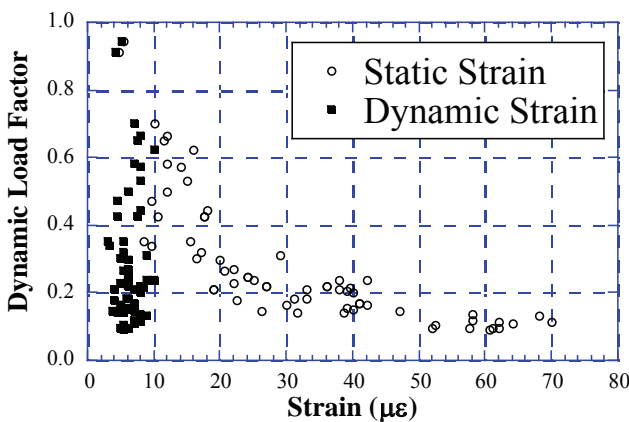


Fig. 8. Strain vs. dynamic load factor

To verify dynamic load the fallow measurement should be done on the bridge: dynamic load amplification, corresponding truck weight, in particular axle loads and axle spacing. The measurements should be taken simultaneously by two systems: the weight-in-motion (WIM) system and dynamic system (accelerations). The WIM system is purpose to measure and record all relevant

truck information in addition to the strain response in each girder. The dynamic system is set up to measure accelerations simultaneously in this same location, where the strain gauges (close to maximum moment) [Nassif and Nowak 1995].

These measurements carry out static and dynamic stresses for each girder. The test results are showing that dynamic component of stresses is practically independent of static component. Therefore, verification of dynamic load on existing bridges is very important.

4.4. Fatigue load spectra

Fatigue is an important consideration in the design and analysis of steel bridge structures. Multiple passages of heavy trucks can lead to cracking and premature failure. Analysis of fatigue performance involves the determination of loads and material strength. Material response has been studied by many researchers. Fisher (1983) developed S-N curves for categories of details in steel structures. Fisher's work demonstrated the importance of load level, particularly magnitude and frequency of occurrence. For example, many fatigue load tests for girder bridges were conducted by Laman and Nowak (1996).

The objective of fatigue load research has largely been to establish an equivalent fatigue truck that will cause the same cumulative fatigue damage as the normal traffic distribution. A single, equivalent fatigue truck is a very attractive and useful tool for the practicing engineer. Schilling (1984), Raju et al (1990), and AASHTO (1989) suggest that the accuracy of the fatigue truck model is improved by adjusting the fatigue truck axle weights in proportion to an equivalent total weight, calculated from the specific site load distribution. In addition to the equivalent total weight, the equivalent lane moment has been calculated for each bridge in the study, which may be a more accurate indication of Miner's equivalent stress for use in fatigue calculations, particularly for shorter (< 20 m) spans. The equivalent lane moment does not, however, include the effects of intermediate smaller cycles caused by long vehicles crossing the bridge or dynamic effects. Greater accuracy is achieved when these intermediate cycles are included in the fatigue analysis.

In test conducted by Jeffrey and Nowak in 1996, a fatigue load model was developed from weigh-in-motion (WIM) measurements [Laman 1995]. Statistical parameters of stress were calculated for girder bridges. The results indicated that magnitude

and frequency of truck loading were strongly site-specific and component-specific. Based on the WIM data, a design fatigue truck was developed. The model was calibrated against measured dynamic strains to achieve uniform reliability against fatigue failure.

The tests show that live load stress spectra are strongly component-specific. Each component experiences a very different distribution of strain cycle ranges. The girder that is nearest the left wheel track of vehicles traveling in the right lane experiences the highest stresses in the stress spectra and decreases as a function of the distance from this location. This information can be useful to target bridge inspection efforts to the critical members.

Example of the results of measurements taken on the bridge with 9 girders is presented in Figure 9. The cumulative distribution functions are shown for each girder. For this bridge, the response of each girder to the live load varies considerably.

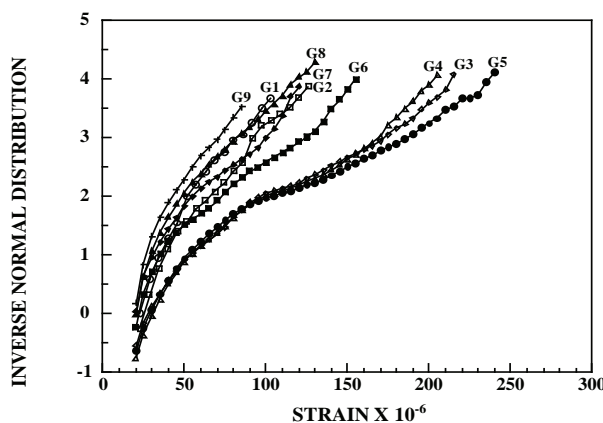


Fig. 9. CDF's of strain for different girders

A vehicle type that dominates the distribution of vehicle types does not necessarily dominate the fatigue damage of the particular component. A vehicle type that dominates the distribution of lane moments will likely dominate the fatigue analysis. This has been demonstrated in this study by the ten and eleven axle vehicles at each bridge and for several span lengths. Eleven axle vehicles dominate the extreme values of the load spectra. Distributions of lane moment demonstrate that eleven axle vehicles, although longer with more even load distribution, produce lane moments that are much greater than 5 axle vehicles.

The fatigue load models based on a three axle truck may overestimate the fatigue damage for bridges with a simple span shorter than 12 to 18 m and underestimate the fatigue damage for longer spans. The proposed fatigue load model more accurately predicts the fatigue damage caused by normal truck

traffic passing over a bridge. The model is site-specific and is characterized by the load spectra of the bridge.

4.5. Proof load testing

To estimate the inherent extra capacities of bridges, several nondestructive load tests have been in use for many years. In general, nondestructive load test can be divided in two categories: diagnostic tests and proof load tests. Diagnostic tests are performed to get a better understanding of the bridge behavior, whereas proof load tests are used to obtain the actual live load capacity or to check the ability of the bridge to carry a certain live load with a factor of safety [Saraf, Sokolik and Nowak 1997].

Diagnostic tests involve a lower load level such as small trucks or normal traffic, and are used to calibrate or verify analytical models. These analytical models are then used to calculate the rating factors. However, several important parameters influencing the bridge behavior at lower load levels, such as the unintended composite action, bearing restraints, and effect of parapets, may disappear at higher load levels. Alternatively, proof load testing can be used for accurate evaluation of load-carrying capacity [Saraf and Nowak 1998].

Proof load testing can be used either to find the yield capacity of the structure, or to check its ability to carry a specified live load. Usually, the yield capacity of a bridge is very high and requires exceptionally heavy loads. In study [Saraf and Nowak 1998], proof load tests were carried out to verify if the bridge can safely carry the maximum allowable legal load. In Michigan, the maximum midspan moment in medium span bridges is caused by two-unit 11-axle trucks [Michigan Bridge Analysis Guide 1983]. For such an 11-axle truck, GVW can be up to 685 kN, which is almost twice the allowable legal load in other states (most states allow a maximum GVW of only 356 kN), more than five times the H15 design load, and more than twice the HS20 design load.

The proof load level should be sufficiently higher than that from a two-unit 11-axle truck to ensure the desired level of safety [Lin and Nowak 1984]. Until recently, the calculation of the appropriate proof load level was left to the judgment of researchers conducting the test. The final draft report by Lichtenstein (1993) provides guidelines for calculating the target proof load level. It suggests that the maximum allowable legal load should be multiplied by a factor X_p , which represents the live load factor needed to bring the bridge to an operating rating factor of 1.0. The report

recommends that X_p should be 1.4. It also recommends several adjustments to X_p , which should be considered in selecting a target live load magnitude. According to the report, testing load should cause twice bigger effect than allowable legal load.



Fig. 10. Proof load test of a bridge using military tanks

5. Conclusions

Experimental procedures can be used as an efficient tool in evaluation of structures in particular when combined with analytical methods. There is a variety of equipment of techniques available for a wide spectrum of applications. The major selection criteria depend on what is to be measured, observed or monitored. The requirements and considerations include:

- Accuracy. Strain in steel and concrete is typically measured in terms of 0.001 or less, while deflection in 0.1 inch (or less). Higher accuracy can be costly.
- Ease of installation. This is an important consideration, as installation can be time-consuming, costly and disruptive to normal operation of the structure.
- Ease of operation. The equipment that runs without any operator is preferred, but it has to be reliable as frequent repairs can be costly.
- Time frame for operation of equipment. There is considerable difference between a short-term (seconds, minutes, hours, days, weeks) and long-term (weeks, months, years).
- Economics. Application of diagnostic procedures is viable when their cost is below the expected cost of repairs or replacement.
- On-site power supply. Availability of power supply can be detrimental in particular in case of long-term measurements. Renewable sources (e.g. solar or wind) can be considered as alternative solutions.
- Environmental effects. There are two groups issues. One is the effect of ambient conditions (weather, temperature, rain, snow, ice, wind, water) on

functioning of the diagnostic equipment. The other is environmental protection restrictions which can impact the practical applicability of a procedure.

- Days and hours of operation. The availability of equipment and/or access to the structural components can be restricted to certain time periods, e.g. nights or after work hours only.
- Closure, limited operation and traffic control. In transportation projects, a major consideration is avoidance of any traffic disturbance such as lane closure, bridge closure or detour. Otherwise, there is an inconvenience to the public and increased risk of traffic accidents. Traffic control is also an additional cost that is added to the budget of diagnostic procedures.
- Security issues. Diagnostic procedures can make the structure vulnerable to vandalism or terrorist attack. Therefore, it is safe to consider the security issues when planning diagnostic testing.
- New developments. The new devices and techniques become available and it is important to keep track of the new developments that need to be checked for structural monitoring and diagnostics {note: this is obvious, so the suggestion}.

References

- [1] Bakht B., and Jaeger L.G.: *Bridge Testing – A Surprise Every Time* ASCE Journal of Bridge Engineering, Vol. 116, No. 5, May 1990, pp. 1370-1383.
- [2] Hellier C.: *Handbook of nondestructive evaluation*, McGraw-Hill, 2001, New York.
- [3] Abudayyeh O., Abdel-Qader I., Nabulsi S., and Weber J.: *Using nondestructive technologies and methods in bridge management systems*. J. Urban Technol., Vol. 11, No. 1, 2004, pp. 63-76.
- [4] Merkle W., Myers J.J.: *Use of the total station for serviceability monitoring of bridges with limited access in Missouri, USA*. Center of Infrastructure Engineering Studies (CIES), Department of Civil Engineering, University of Missouri-Rolla, USA.
- [5] Blitz J., Simpson G.: *Ultrasonic Methods of Non-Destructive Testing*. Springer - Verlag New York, LLC, 1991.
- [6] ASTM: *Standard test method for measuring the P-wave speed and thickness of concrete plates using the impact-echo method*. Annual book of ASTM standards, C 1383, Farmington Hills, Michigan, 1998, Vol. 04.02.
- [7] Ming-Cheng Chen, Chin-Kuo Huang and Chung-Yue Wang: *Crack Condition Evaluation Approach for the Deteriorated Girder of an RC Bridge*. ASCE Journal of Bridge Engineering, Vol. 12, No. 5, 2007, pp. 654-661.

- [8] AASHTO LRFD, Bridge Design Specifications, American Association of State Highway and Transportation Officials, Washington, D.C., 1998.
- [9] Eom J., Nowak A.S.: *Live Load Distribution for Steel Girder Bridges*. ASCE Journal of Bridge Engineering, Vol. 6, No. 6, 2001, pp. 489-497.
- [10] Kim S.J., Nowak A.S.: *Load distribution and impact factors for I-girder bridges*. ASCE Journal of Bridge Engineering, Vol. 2, No. 3, 1997, pp. 97-104.
- [11] Nowak A.S., Eom J. Sanli A. and Till R.: *Verification of Girder Distribution Factors for Short-Span Steel Girder Bridges by Field Testing*. Transp. Research Record, No. 1688, 1999, pp. 62-75.
- [12] Nowak A.S., Kim S-J., Stankiewicz P.R.: *Analysis and Diagnostic Testing of a Bridge*. Journal of Computers and Structures, 77, 2000, pp. 91-100.
- [13] Nassif H. Nowak A.S.: *Dynamic Load Spectra for Girder Bridges*. Transportation Research Record, No. 1476, 1995, pp. 69-83.
- [14] AASHTO Standard Specifications for Highway Bridges, American Association of State and Transportation Officials, Washington, DC, 2002.
- [15] AASHTO LRFD, Bridge Design Specifications, American Association of State Highway and Transportation Officials, Washington, D.C., 2007.
- [16] Nassif H., Nowak A.S.: *Dynamic Load for Girder Bridges under Normal Traffic*. Archives of Civil Engineering, Vol. XLII, No. 4, 1996, pp. 381-400.
- [17] Fisher J.W., Mertz D.R., Zhong A.: *Steel Bridge Members Under Variable Amplitude Long Life Fatigue Loading*. NCHRP Report 267, TRB, Washington D.C., December 1983.
- [18] Laman J.A., Nowak A.S.: *Fatigue-Load Models for Girder Bridges*. ASCE Journal of Bridge Engineering, Vol. 122, No. 7, July 1996, pp. 726-733.
- [19] Schilling C.G.: *Stress Cycles for Fatigue Design of Steel Bridges*. ASCE Journal of Bridge Engineering, Vol. 110, No. 6, June 1984.
- [20] Raju S.K., Moses F., Schilling C.G.: *Reliability Calibration of Fatigue Evaluation and Design Procedures*. Journal of Structural Engineering, Vol. 116:1356-69, May 1990.
- [21] AASHTO Guide Specification for Strength Evaluation of Existing Steel and Concrete Bridges, American Association of State Highway and Transportation Officials, Washington, D.C, 1989.
- [22] Jeffrey A.L., Nowak A.S.: *Fatigue load model for girder bridges*. ASCE Journal of Bridge Engineering, Vol. 122, No. 7, 1996, pp. 726-733.
- [23] Laman J.A.: *Fatigue Load Models for Girder Bridges*, Doctoral Dissertation, University of Michigan, Ann Arbor, MI. 1995.
- [24] Saraf V., Sokolik A.F., Nowak A.S.: *Proof Load Testing of Highway Bridges*. Transportation Research Record, No. 1541, 1997, pp. 51-57.
- [25] Saraf V., Nowak A.S.: *Proof Load Testing of Deteriorated Steel Girder Bridges*. ASCE Journal of Bridge Engineering, Vol. 3, No. 2, May 1998, pp. 82-89.
- [26] Michigan Bridge Analysis Guide. Michigan Department of Transportation, Lansing, 1983.
- [27] Lin T.S. Nowak, A.S.: *Proof Loading and the Structural Reliability*. The Journal of Reliability Engineering, Vol. 8, No. 2, 1984, pp. 85-100.
- [28] Lichtenstein A.G.: *Bridge rating through nondestructive load testing*. NCHRP Project 12-28 (13) A final draft. TRB, National Research Council, Washington D.C., June 1993.

GRZEGORZ MAZUREK

Kielce University of Technology
Faculty of Civil and Environmental Engineering
al. Tysiąclecia Państwa Polskiego 7
25-314 Kielce, Poland
e-mail: gmazurek@tu.kielce.pl

THE ASSESSMENT OF THE RESILIENT MODULUS OF ELASTICITY OF ASPHALT CONCRETE WITH LOW-VISCOSITY MODIFIER

Abstract

Based on the experiments it was found that the operating temperature significantly influenced the resilient modulus of elasticity of asphalt concrete. The study was intended for asphalt concrete used for the wearing course AC 11 S. In the experiment bitumen 35/50 was used which was modified with synthetic wax (Fisher-Tropsh) in the range of 1.5% - 4.0% with steps every 0.5%. The asphalt concrete has been compacted at the optimum characteristic temperature of 125°C. The study revealed a low susceptibility of temperature of asphalt concrete with asphalt low-viscosity in the range of 5°C to 25°C. In addition a negative impact of the lack of compaction level on resilient modulus of elasticity of the asphalt concrete was found.

Keywords: resilient modulus of elasticity, surface, synthetic wax.

1. Introduction

The increase in requirements in relation to the load of road surfaces is a result of increasing level of maximum wheel load that is transmitted to the ground and destruction of roads exaggerated by a climatic factor [1]. An important element in lowering the bearing capacity of pavement is decreasing a compaction temperature in the autumn season. Possible solution of this problem is the use of mineral mix asphalt produced in the "warm technology" (WMA). The implementation of asphalt concrete in such technologies requires modification of the viscosity of the binder by foaming or chemical modification. Chemical modification is done by using synthetic waxes which can substantially reduce the level of viscosity of asphalt at temperatures above 110°C. An additional advantage of this type of technology is an improved characteristics of visco-elastic asphalt concrete bears on a resilient modulus of elasticity expressed by a thermal susceptibility of the material. Analysis of a resilient modulus of elasticity according to EN 12697-26 [2], in particular temperature ranges, gives a chance of

quick evaluation of excessive stiffness of the asphalt concrete leading to the reduction in fatigue life. The study of a resilient modulus of elasticity broadens knowledge of the potential rutting of the asphalt concrete.

2. Dynamic viscosity of low-viscosity bitumen

The tests of the impact of the low-viscosity modifier on changes of the bitumen properties were conducted for the traditional 35/50 bitumen. This binder was modified by low-viscosity modifier in the range of 1.5% to 4.0% with steps every 0.5% in relation to the amount of the bitumen. The samples were blended according to the condition of production [3]. Dynamic viscosity expresses the internal friction which occurs due to the existence of cohesion forces between the constituents of bitumen as they move relative to each other [4]. The viscosity of bitumen was measured at a shear rate of 1 s^{-1} . The viscosity measurement was carried out in three specific temperatures 60°C, 90°C and 135°C.

The changes of dynamic viscosity as a function of temperature have been presented in Figure 1.

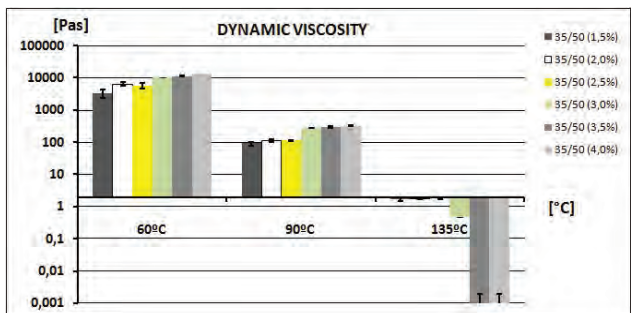


Fig. 1. Dynamic viscosity versus temperature

The results show that as the content of the low-viscosity modifier increases, there is a considerable diversity in the measurement of dynamic viscosity of bitumen at medium temperatures. It should be noted that as the temperature increased the dynamic viscosity of the bitumen decreased. With the increasing amount of low-viscosity modifier up to 90°C the dynamic viscosity still increased. In particular at the temperature 60°C stiffening of the bitumen will have a positive effect on the resistance to forming permanent deformation. It must be linked to an increase of the resilient modulus of elasticity. The fact of stiffening of the bitumen as well as an increase in viscosity will depend on the level of crystallization of paraffin in wax. The increase of stiffening of low-viscosity bitumen, on a smaller scale, is reproduced at 90°C, which generates a conclusion that there is a strong plate lattice of micro crystalline paraffins in bitumen. At the temperature of 135°C the situation changed. This time the increase of the wax content caused radical reduction of the viscosity below 2 Pa·s, which was adopted as a necessary viscosity level of optimal covering aggregate. To make observation easier, values of dynamic viscosity were presented in a semi-logarithmic scale. The value of dynamic viscosity of 2 Pa·s was presented as the main axis of the domain. It can be concluded that the temperature of 135°C is sufficient to ensure the optimum viscosity level of covering aggregate. It must be noted that the temperature of compaction could be decreased down to 30°C which is necessary for proper compaction of the asphalt concrete in the range of viscosity between 2 to 20 Pa·s [5]. The proper compaction of the asphalt concrete also affects the resilient modulus of asphalt concrete.

3. Methodology and test results analysis of resilient modulus of asphalt concrete with low-viscosity modifier

The experiment was carried out on asphalt concrete AC 11 S which was designed for wearing course layer in accordance with PN EN 13108-1. The reference asphalt concrete which constrained the main aggregate

of quartzite in the amount of 55% was designed. A dolomite mix 0/4 in the amount of 24% and granite fractured sand were used to increase fraction contents. The modification of asphalt synthetic wax was made in the amounts of 1.5%, 2.0%, 2.5%, 3.0%, 3.5%, 4.0% by weight, in proportion to 35/50 virgin bitumen [3].

During the determining process of these parameters, an important element of research was to evaluate the homogeneity of the work. The study allows only a sample, in which the voids in the group ranged within outliner results in line with the Grubbs test [6, 7].

The experiment was realized according to the research program within the confines of two factorial design of experiment. Fitted statistically significant model was a polynomial of the second degree [8, 9]. The fixed factors were set as the amount of low-viscosity modifier (L_V) and operation temperature (TEMP). Void fraction content (Wp) was a quantitative and random factor. The visual characteristic of variation of resilient modulus of elasticity, as a regression model, have been presented in Figure 2.

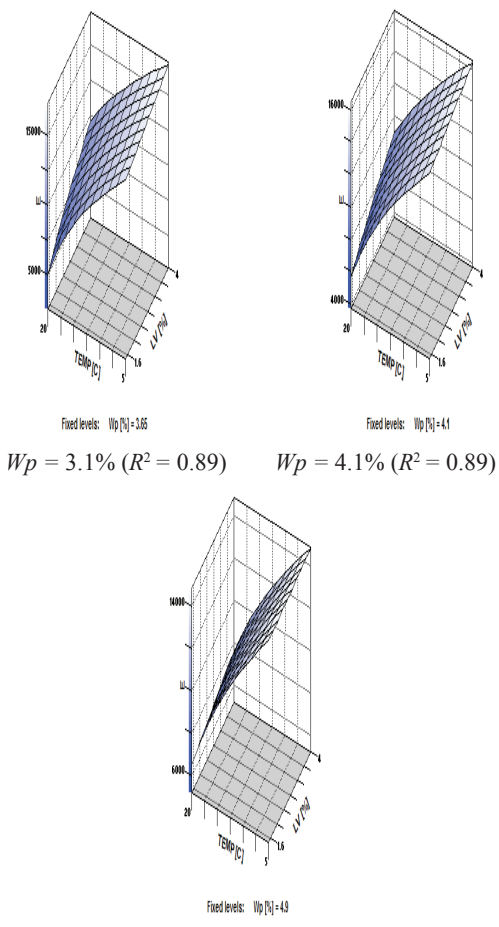


Fig. 2. Resilient modulus of elasticity versus operational temperature and low-viscosity modifier

It should be noted that the amount of low-viscosity modifier had a statistically significant influence on the resilient modulus of elasticity (p -value = 0.0215), as the amount of low-viscosity modifier increased. However, the greatest changes in the level the resilient modulus of elasticity were observed during changing of the operate temperature (p -value < 0.001). This situation is related to the level of crystallization of aliphatic modifier, which in turn can lead to excessive stiffening of asphalt concrete. The void fraction content had a relevant influence. The highest resilient modulus of elasticity values were registered when the level of void fraction content was in the range of 3.0 and 3.5%. The constant increase in void fraction content, revealed as a lack of proper compaction, resulted in lowering the resilient modulus of elasticity especially at 25°C. This situation may affect the ability of constant compaction of asphalt concrete and it is the beginning of rut forming process at higher temperatures. Additionally, the excess void fraction content causes the marginalization of the effect of the modifier, as can be seen for void fraction content of 4.9%. Thus, the impact of the lack of rigor in the compaction process eliminates the benefits of using synthetic wax.

Resilient modulus of elasticity depends on the time of loading and temperature measurement. To further analyze the test results an assessment of the thermal susceptibility of the resilient modulus of elasticity of asphalt concrete with asphalt low-viscosity modifier. The study was conducted for the Marshall samples in temperature ranges of 5°C, 12°C and 25°C, all of them have been compacted at the optimum temperature of 125°C [5]. The temperature of 12°C is accepted as equivalent in the Polish standard and it is a level of visco-elastic characteristics as accepted to the mechanistic designing method. The results of the dynamics of the expected and predicted value of resilient modulus of elasticity in term of the temperature (performed in SAS) have been presented in Figure 3.

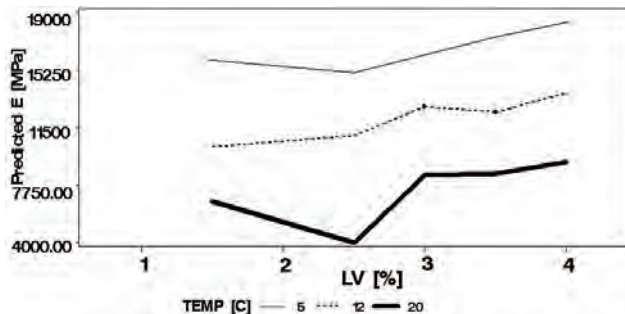


Fig. 3. Predicted value of resilient modulus of elasticity versus the content of low-viscosity modifier (L-V) and operational temperature (TEMP)

Analyzing the growth rate of the stiffness, it should be noted that the proportional growth rate in relation to the level of the measurement temperature. The slope angle of trend growth of the x-axis is similar for different temperatures without the impact of the dosage of the low-viscosity modifier. It can be concluded that a low dosage of the modifier in the amount of 4% did not cause a sudden increase in stiffening of the asphalt compared to other variants of dosage. Thermal susceptibility of low-viscosity bitumen with different variants of dosage of synthetic wax will not cause an excessive increase in the complex viscosity of asphalt concrete. The level of resilient modulus of elasticity will proportionally vary depending on the amount of the modifier concentration.

4. Conclusions

Based on the analysis of the test results of asphalt concrete the following conclusions can be drawn:

- the increase in the amount of synthetic wax causes the stiffening of the bitumen at operating temperatures below 60°C and significant liquidation at 135°C;
- the measurement of both temperature and amount of the low-viscosity modifier significantly affect the resilient modulus of elasticity. In relation to the dynamics, the temperature measurement had the greatest influence;
- excessive void fraction content significantly limited the beneficial stiffening effect of the modifier;
- thermal susceptibility of the asphalt concrete with the low-viscosity modifier remains at a similar level in the modifier dosage up to 4%.

References

- [1] Stefańczyk B., Mieczkowski P.: *Mineral mix asphalt*, WKiŁ, Warsaw 2008.
- [2] PN-EN 12697-26:2004 Hot mix asphalt - requirements – Test methods for hot mix asphalt: Stiffness.
- [3] Product Information, The Bitumen Additive for Highly Stable Easy Compactable Asphalts, 2008.
- [4] Gaweł I., Kalabińska M., Piłat J.: *Asfalt drogowy* [Road bitumen], WKŁ, Warsaw, 2001
- [5] Iwański M., Mazurek G.: *Asphalt concrete of low-viscosity modifier*, 2nd International Conference on Transport Infrastructures in São Paulo, Brazil, August 2010.
- [6] Grubbs F.E.: *Procedures for detecting outlying observation in samples*, Technometrics, Vol. 11, No 1, p 1-21, February 1969.
- [7] Guide to Expression Uncertainty in Measurement, ISO Switzerland 1995.
- [8] Piasta Z., Lenarcik A.: *Methods of statistical multi-criteria optimisation*, [in:] A.M. Brandt (ed.), Optimization Methods for Material Design of Cement based Composites, E & FN Spon, London, New York, 1998, pp. 45-59.
- [9] Montgomery D.G., *Design and Analysis of Experiments*, 5th Edition, John Wiley and Sons, 2001.

Grzegorz Mazurek

Badania modułu sztywności sprężystej betonu asfaltowego z asfaltem niskowiskozowym

1. Wstęp

Wzrost wymagań w odniesieniu do obciążen nawierzchni drogowych wynika ze wzrostu poziomu maksymalnego obciążenia ruchem ulicznym przekazywanego do gruntu i niszczenia dróg, co dodatkowo pogarsza wpływ czynników klimatycznych [1].

2. Lepkość dynamiczna asfaltu niskowiskozowego

W badaniach wpływu modyfikatora niskowiskozowego na zmiany właściwości asfaltu zastosowano jako lepiszcze asfalt zwykły 35/50 pochodzący z Petrochemii w Płocku. Modyfikator dozowano w przedziale od 0,5% do 4,0% w stosunku do masy asfaltu 35/50 zwiększąc jego ilość o 0,5%. Próbki zostały wykonane w blenderze symulując warunki wykonania zgodnie z [3]. Lepkość dynamiczna wyraża tarcie wewnętrzne występujące w wyniku istnienia sił kohezji między składnikami grupowymi przy przesuwaniu jednej warstwy asfaltu względem drugiej [4]. Do badań wykorzystano lepkościomierz obrotowy typu „Rheotest 2” z układem cylindrów współosiowych typu H2. Wszystkie lepkości asfaltów zostały zmierzone przy szybkości ścinania wynoszącej 1 s^{-1} . Pomiar lepkości był realizowany w zakresie temperatur 60°C , 90°C i 135°C . Zmiany lepkości w funkcji temperatury przedstawiono na rysunku 1.

Wyniki badań wskazują, że w miarę wzrostu modyfikatora niskowiskozowego. Występuje duże zróżnicowanie w pomiarze lepkości dynamicznej w średnich. Należy zwrócić uwagę, że w miarę wzrostu temperatury następuje obniżenie lepkości dynamicznej asfaltu. W miarę wzrostu ilości modyfikatora niskowiskozowego w zakresie do 90°C następuje wzrost lepkości. Szczególnie w temperaturze 60°C usztywnienia asfaltu będzie miał korzystny wpływ na odporność takiej mieszanki na powstawanie odkształceń trwałych. Przy takim stanie rzeczy należy się spodziewać wzrostu modułu sztywności sprężystej. Fakt usztywnienia asfaltu jak i również wzrost lepkości będzie uzależniony od poziomu krystalizacji parafin twardych w woskach. Wzrost usztywnienia asfaltu przez modyfikator niskowiskozowy, choć w mniejszej skali, jest powielony w temperaturze 90°C , co generuje wniosek, że nadal w asfalcie istnieje silna sieć krystaliczna węglowodo-

rów parafinowych. W temperaturze 135°C sytuacja ulega zmianie. Tym razem wzrost zawartości wosków powoduje diametralne obniżenie lepkości poniżej $2 \text{ Pa}\cdot\text{s}$, czyli poziomu przyjętego jako optymalny otaczania kruszywa. Dla ułatwienia obserwacji wartości lepkości przedstawiono w skali półlogarytmicznej. Wartość lepkości dynamicznej wynoszącej $2 \text{ Pa}\cdot\text{s}$ przedstawiono jako oś główną dziedziny. Można stwierdzić, że temperatura 135°C jest wystarczająca do zapewnienia optymalnego poziomu lepkości niezbędnej do otoczenia kruszywa. W miarę wzrostu dozowania modyfikatora można obniżyć poziom temperatury nawet o 30°C która jest niezbędna do prawidłowego zagęszczenia mieszanki w przedziale od 2 do $20 \text{ Pa}\cdot\text{s}$ [5]. Należy zwrócić uwagę, że właściwe zagęszczenia betonu asfaltowego rzutuje bezpośrednio na poziom modułu sztywności sprężystej.

3. Metodologia oraz analiza wyników modułu sztywności sprężystej betonu asfaltowego z asfaltem niskowiskozowym

W celu oceny wpływu ilości modyfikatora niskowiskozowego na właściwości betonu asfaltowego badania wykonano na betonie asfaltowym o uziarnieniu 0/11 mm przeznaczonym na warstwę ścierową nawierzchni obciążonej ruchem KR4 zgodnie z PN-EN 13108-1. Zaprojektowano beton asfaltowy referencyjny z kruszywem głównym kwarcytowym w ilości 52%. Jako kruszywo doziarniające zastosowano mieszankę dolomitową 0/4 w ilości 24% oraz piasek łamany granitowy 19%. Modyfikację asfaltu woskiem syntetycznym dokonano w ilościach 1,5%, 2,0%, 2,5%, 3,0%, 3,5%, 4,0% wagowo, w stosunku do asfaltu 35/50 na bazie którego wykonano beton asfaltowy [3].

Podeczas określania wyżej wymienionych parametrów, istotnym elementem badań była ocena jednorodności wykonywanych prac. Do badań przyjmowano tylko próbki, w których zawartość wolnych przestrzeni w danej grupie zawierała się w przedziale wyników nieodstających zgodnie z założeniami testu Grubbsa [6, 7].

Doświadczenie realizowano zgodnie z programem badań opracowanym na podstawie trójczynnikowego planu eksperymentu. Istotnym statystycznie mo-

delem dopasowania okazał się wielomian drugiego stopnia [8, 9]. Jako elementy stałe jakościowe ustalonej zawartość modyfikatora niskowiskozowego (L_V) oraz temperaturę pomiaru (TEMP). Zawartość wolnych przestrzeni (W_p) miała charakter ilościowy i losowy. Wizualny charakter przebiegu zmienności cechy modułu sztywności sprężystej w formie modelu regresyjnego powierzchni odpowiedzi przedstawiono na rysunku 2.

Należy zwrócić uwagę, że w miarę wzrostu ilości modyfikatora nisko- wiskozowego ($p\text{-value} = 0,0215$) następuje istotny statystycznie wzrost poziomu modułu sztywności sprężystej. Jednak największy poziom zmian modułu sztywności sprężystej zanotowano przy zmianie poziomu temperatury pomiaru ($p\text{-value} < 0,001$). Taka sytuacja jest związana z poziomem kryształizacji węglowodorów alifatycznych modyfikatora, co w konsekwencji może doprowadzić do nadmiernego przesztywnienia betonu asfaltowego. Zawartość wolnych przestrzeni nie była tu bez znaczenia. Najwyższe wartości modułu sztywności sprężystej zanotowano przy zawartości ilości wolnych przestrzeni w zakresie 3,0 do 3,5 %. Dalszy wzrost wolnych przestrzeni, czyli brak właściwego zagęszczenia, skutkował obniżeniem modułu sztywności sprężystej szczególnie w temperaturze 25°C. Taka sytuacja może rzutować na możliwość samodogęszczania betonu asfaltowego oraz początek powstawania kolejnych w wyższych temperaturach eksploatacyjnych. Dodatkowo nadmierna zawartość wolnych przestrzeni powoduje marginalizację efektu modyfikatora, co można zauważyć na regresji dla maksymalnej zawartości wolnych przestrzeni wynoszącej 4,9%. Zatem wpływ braku rygoru podczas zagęszczania eliminuje korzyści wynikające z zastosowania wosku syntetycznego.

Moduł sztywności sprężystej zależy od czasu obciążenia oraz temperatury pomiaru. Celem dalszej analizy wyników badań była ocena podatności termicznej modułu sztywności betonu asfaltowego z asfalem niskowiskozowym. Badanie przeprowadzono dla próbek zagęszczanych sposobem Marshalla badanych w trzech zakresach temperaturowych: 5°C, 12°C oraz 25°C przy czym wszystkie zostały zagęszczane w temperaturze optymalnej 125°C [5]. Temperatura 12°C jest przyjmowana w Polsce jako równoważna i dla jej poziomu w projektowaniu przyjmowane są charakterystyki lepko-sprężyste w metodzie mechanistycznej. Wyniki dynamiki zmian oczekiwanej wartości prognozowanego modułu sztywności sprężystej w zależności od temperatury badania (wykonane w programie SAS) przedstawiono na rysunku 3.

Analizując tempo wzrostu modułu sztywności sprężystej należy zwrócić uwagę na proporcjonalny poziom wzrostu badanej cechy w odniesieniu do temperatury pomiaru. Kąt nachylenia wzrostu do osi x jest zbliżony dla różnych temperatur bez względu na poziom ilości modyfikatora niskowiskozowego. Można stwierdzić, że dozowanie modyfikatora niskowiskozowego w zakresie do 4% nie spowoduje nagłego przyrostu usztywnienia asfaltu w stosunku do innych wariantów dozowania. Wrażliwość termiczna asfaltu niskowiskozowego z różnymi wariantami ilości wosków syntetycznych nie spowoduje nadmiernego przyrostu ogólnej lepkości betonu asfaltowego. Poziom modułu sztywności sprężystej będzie zmieniał się proporcjonalnie w zależności od ilości modyfikatora nisko- wiskozowego.

4. Wnioski

Na podstawie przeprowadzonych badań sformowano następujące wnioski:

- wzrost ilości wosków syntetycznych powoduje usztywnienie asfaltu w temperaturach eksploatacyjnych poniżej 60°C oraz znaczne upłynnienie w temperaturze 135°C;
- zarówno temperatura pomiaru jak ilość modyfikatora niskowiskozowego istotnie statystycznie wpływają na zmiany modułu sztywności sprężystej. W odniesieniu do dynamiki to temperatura pomiaru odznacza się największym wpływem;
- nadmierna zawartość wolnych przestrzeni znacznie marginalizuje korzystny wpływ usztywnienia asfaltu modyfikatorem niskowiskozowym;
- wrażliwość termiczna betonu asfaltowego modyfikowanego woskiem syntetycznym pozostaje na zbliżonym poziomie w zakresie dozowania modyfikatora 4%.

ZDZISŁAWA OWSIAK¹

JUSTYNA ZAPALA²

Kielce University of Technology
Faculty of Civil and Environmental Engineering
al. Tysiąclecia Państwa Polskiego 7
25-314 Kielce, Poland

¹e-mail: owsiaak@tu.kielce.pl

²e-mail: j.zapala@tu.kielce.pl

REVIEW OF THE LABORATORY METHODS APPLIED TO ASSESS THE REACTIVITY OF ALKALINE SILICEOUS AGGREGATES IN CONCRETE

Abstract

The alkali-silica reaction is one of those reactions that cause the concrete destruction. The question of the alkali-aggregate reaction has not been fully explained as yet. This paper presents the outline of the reaction mechanism, and discusses the most common methods of investigating the reactivity of aggregates and of aggregate-cement mixtures. The ideal testing method should be fast, simple, precise and accurate. None of the accessible methods combine all those assumptions. The paper presents the evaluation of the applied methods.

Keywords: alkali-silica reaction, aggregate, testing methods.

1. Introduction

The expansion processes resulting from the alkali-aggregate reaction leads to both the utilitarian and the aesthetic values of the buildings being decreased. The reaction is slow, therefore its destructive effects become evident only after a longer period of time. The progress of the alkali-aggregate reaction depends on many factors, i.a. on the composition of concrete pore solution and on the presence of reactive aggregate.

Thus the evaluation of the aggregate reactivity appears to be necessary before its application in real life structures. The probability of the reaction can be determined by direct analysis tests performed on aggregates and by indirect analysis of the standard mortar and concrete samples.

2. Mechanism of alkali-silica reaction [1]

The alkali-silica reaction takes place between reactive components of silica aggregates and alkalis present in cement. In order for the reaction to take place there must be favourable conditions: high moisture, high pH and the reactive silica. The reactive silica reacts with hydroxyl groups present in the concrete pore solution. The effect of sodium and potassium ions on the silica grain results in the destruction of the three-dimensional structure of quartz. This process gives polymineral gel,

which is capable of absorbing water and thus of giving an expansive product. The resultant gel is surrounded by mortar components and therefore an osmotic pressure is generated. This pressure exceeds the tensile strength of concrete, which consequently leads to concrete cracking. As the water content grows, the resultant gel can move in concrete, filling pores and cracks.

3. Methods of testing the occurrence of the alkali-silica reaction

Petrographic and chemical methods can be distinguished among the most common methods evaluating the alkali-aggregate reactivity, both according to American standards ASTM and European standards RILEM.

The testing of the alkali-aggregate reactivity is performed through:

- aggregate petrographic analysis,
- mortar and concrete samples analysis in ultra-fast laboratory tests,
- mortar and concrete samples analysis in long-term tests.

3.1. Aggregate petrographic analysis

American method ASTM C295 [2] uses the following petrographic techniques to evaluate

siliceous aggregate reactivity: optical microscopy, energy-dispersive X-ray spectroscopy (EDS) and X-ray powder diffraction (XRD) infrared spectroscopy, and thermic analysis. The analysis is performed on samples in the form of core samples, cross-sectional samples or pieces of aggregate. The analysis of the obtained picture permits primarily the qualitative determination of minerals (optical microscopy), and their quantitative determination, detection of voids, defining the size and shape of grains (computer analysis of the picture).

As far as silica aggregates are concerned, the reactive minerals include: opal, cristobalite, tridymite, obsidian, siliceous glass, horn-stone, chalcedony, cryptocrystalline volcanic rocks i.e. andesite, rhyolith, metamorphic quartz under stress and microcrystalline silica [3].

Petrographic methods permit identifying reactive forms of silica, however, it is a difficult task due to the difficulties in identifying particular forms. Thus it is one of the reasons for applying dilatometric methods in order to evaluate the aggregate reactivity and for combining them with petrographic methods. Although this test cannot provide information on the behaviour of aggregate in the presence of alkalis from cement, it permits choosing an appropriate accelerated method, a further method of testing the aggregate reactivity.

RILEM AAR1 [4] recommends microscopic testing of aggregate samples reactivity, based on: separating particles and observing their cross section (this procedure is relatively uncertain and inappropriate for examining unknown or complex aggregates), spot testing (considered to be the most accurate of the methods) and the whole-rock petrography. On the basis of the tests the aggregates are classified into one of the classes: I – non-reactive aggregates, II – potentially reactive aggregates, III – reactive aggregates.

3.2. The analysis of mortar and concrete samples in ultra-fast laboratory tests

a) the accelerated method ASTM C1260 [5]

The method takes advantage of a feature characteristic of most chemical reactions – the reaction goes faster in higher temperature.

Mortar bars with the dimensions 25x25x250 mm (in RILEM AAR-2 the dimensions are: 40x40x160 mm) [4], with the w/c ratio which equals approximately 0.5, are kept in 1M NaOH solution in the temperature of 80°C. The changes in the samples length are marked on day 4, 7, 11 and 14. The point of reference is the

initial measurement, performed on samples that have been kept for 24 hours in water in the temperature of 80°C. In the ultra-fast method the obtained difference in lengths bigger than 0.1% and smaller than 0.25% indicates a medium reactive aggregate and an expansion of more than 0.25% indicates a very reactive aggregate. At the same time an expansion of less than 0.1% of the initial value indicates a non-reactive aggregate.

In contrast to ASTM C227 – in ASTM C1260 the degree of expansion decreases together with the fall of the w/c ratio (probably the degree of alkali ions migration in the sample goes down). It has also been noted that high temperature and NaOH concentration cause the decrease in calcium ions migration in the material pore solution and consequently the increase in the silica solubility and diffusion from the solution outside. This effect leads to the decrease in the monitored expansion. Thus, the method may produce erroneous results.

According to the conducted tests, ASTM C1260 method gives approximately 36% of falsely negative results [6]. This high number of failures can be reduced by reducing the reactivity criterion from 0.1% to 0.06%, with 14-day tests and 0.13% with tests prolonged to 28 days.

Some researchers of aggregate reactivity have confirmed that it is advisable to prolong the testing time [7].

b) testing mortar samples in a digester

This method is presented as the most promising one for defining the alkali-silica reaction. Mortar samples are prepared according to the ASTM C227 method, however the w/c ratio equals 0.50 and the alkali content equals 3.50% Na₂O_e. The lengths of samples that have been kept in a digester for 5 hours with the pressure of 0.17 MPa and the temperature of approximately 130°C are then measured. It has been concluded that this test is more reliable than the accelerated method ASTM C1260. The suggested expansion time of 0.1% has been recognized as tolerable [8].

c) European standards

According to the European standard AAR-4 (the accelerated method) and AAR-4 Alt. (the alternative method) concrete samples with the dimensions (75±5) x(75±5)x(250±50) mm are stored in the temperature of 60°C. In the AAR-4 method the samples are stored in containers over the water surface, and in the alternative method the samples are wrapped in a wet cotton fabric and polyethylene. The expansion degree

is measured during the period of 20 or 15 weeks. AAR-4 test results showing an expansion higher than 0.03% indicate a reactive aggregate [9].

3.3. The long-term analysis

a) ASTM C227 method [10]

ASTM C227 uses cements with the alkali content of 0.60% of Na_2O_e . The standard does not define the value of the w/c ratio in a very precise way. 24 hours after the molding the bars (25x25x250 mm) are stored at $38^\circ\text{C} \pm 2^\circ\text{C}$ in special containers over the water surface. The lengths measurements of the samples that have been cooled down to the temperature of 23°C are taken after 14 days and then after 1, 2, 3, 4, 6, 9 and 12 months and if necessary also every six months after that. The difference in lengths between the initial sample and the one measured after 12 months bigger than 0.1% permits the conclusion that the aggregate is reactive. The difference smaller than 0.1% indicates the lack of reactivity.

Tests conducted in many centres allowed the researchers to conclude that this test does not make it possible to predict the reactivity in the case of slowly reacting aggregates such as greywacke or argillite [8]. At the same time, the use of containers that are equipped with felt for the storage of samples is connected with washing alkalis out of mortars, which results in the decrease of the expansion grade. Therefore it is believed that the alkali content should be increased to 1.25% and the w/c ratio should not exceed the value of 0.50.

b) the ASTM C1293 method of testing concrete samples [11]

In this method the concrete samples with the dimensions 75x75x285 mm are stored over water, with 100% moisture, in sealed containers and in the temperature of 38°C . The lengths measurements of the samples are taken on day 7, 28, 56 and then after 3, 6, 9 and 12 months and if necessary also every six months after that time. The expansion which after a year's time equals 0.04% means that the aggregate is potentially reactive. The use of this method is significant when petrographic tests have not provided the rationale for claiming that the aggregate is reactive, whereas mortar tests have given the results confirming the reactivity. The long time of duration is undoubtedly a disadvantage of this method.

4. Summary

In the presented methods of testing the potential reactivity of siliceous aggregates, the crucial role is

played by the determinants of the alkali-silica reaction. Because the alkali-silica reaction becomes evident after a longer period of time, increasing parameters such as temperature, pressure, alkali concentration and moisture in the testing methods described in this paper allows the researchers to conclude about the behavior of aggregate in the real structures.

References

- [1] Bernhardsvej C.: *Chemistry of alkali – silica re action and testing of aggregates*. Cement and Concrete Composition, 27 (2005) pp. 788-795.
- [2] ASTM C295. Guide for Petrographic Examination of Aggregates for Concrete. Annual Book of ASTM Standards, Vol. 04.02 (1998).
- [3] Lukschova S., Prikryl R., Pertold Z.: *Petrographic identification of alkali – silica reactive aggregates in concrete from 20th century bridges*. Construction and Building Materials, 23 (2009), pp. 734-741.
- [4] Lindgard J., Nixon P.J., Borches I.: The EU "PARTNER" Project – European standard tests to prevent alkali reaction in aggregates: Final results and recommendation. Cement and Concrete Research, 40 (2010), pp. 611-635.
- [5] ASTM C1260. Standard Test Method for Potential Reactivity of Aggregates (Mortar Bar Method). Annual Book of ASTM Standards, Vol. 04.02 (1993).
- [6] Lenke L.R., Malvar L.J.: *Alkali silica reaction criteria for accelerated mortar bar tests based on field performance data*. 2009 Word of Coal Ash Conference – May 4-7 (2009) in Lexington, USA.
- [7] Chang-Seon Shon, Dan G. Zollinger, Shondeep L. Sarkar.: *Evaluation of modified ASTM C 1260 accelerated mortar bat test for alkali-silica reactivity*. Cement and Concrete Research, 32(2002) 1981-1987.
- [8] Touma W.E.: *Alkali-silica reaction in portland cement concrete: testing methods and mitigation alternatives*. The University of Texas at Austin, (2000), pp.16-26.
- [9] <http://homepage.tudelft.nl/n89v3/Page6.html>.
- [10] ASTM C227: Standard Test Method for Potential Reactivity of Cement – Aggregate Combinations. Annual Book of ASTM Standards, vol. 04.02 (1997).
- [11] ASTM C1293: Standard Test Method for Determination of Length Change of Concrete Due to Alkali Silica Reaction. Annual Book of ASTM Standards, Vol. 04.02 (2002).

Zdzisława Owsiak
Justyna Zapala

Przegląd metod laboratoryjnych stosowanych do oceny reaktywności alkalicznej kruszyw krzemionkowych w betonie

1. Wprowadzenie

Procesy ekspansji będące efektem reakcji alkalia-kruszywo skutkują obniżeniem właściwości użytkowych a także estetycznych budowli. Reakcja jest powolna dlatego jej negatywne skutki ujawniają się dopiero po dłuższym czasie. Postęp reakcji alkalia-kruszywo zależy od wielu czynników spośród których można wymienić skład roztworu w porach betonu oraz obecność kruszywa reaktywnego. Niezbędna staje się więc ocena reaktywności kruszyw przed ich zastosowaniem w rzeczywistych konstrukcjach. Możliwość zachodzenia reakcji można określić stosując testy analizy bezpośredniej, wykonywanej na kruszywach oraz analizy pośredniej na normowych próbках zapraw i betonów.

2. Mechanizmy reakcji alkalia-krzemionka [1]

Reakcja alkalia-krzemionka zachodzi pomiędzy reaktywnymi składnikami kruszyw krzemionkowych a alkaliami zawartymi w cementie. Aby reakcja mogła mieć miejsce muszą wystąpić sprzyjające temu warunki: duża wilgotność, wysokie pH oraz reaktywna krzemionka. Reaktywna krzemionka reaguje z grupami hydroksylowymi obecnymi w roztworze porów betonu. Na skutek działania jonów sodu i potasu na ziarno krzemionki następuje zniszczenie trójwymiarowej struktury kwarcu. Skutkiem procesu jest utworzenie poliminalnego żelu. Żel ten jest zdolny do pochłaniania wody a przez to do tworzenia produktu ekspansywnego. Powstający żel otoczony jest składnikami zaprawy dlatego też dochodzi do wygenerowania ciśnienia osmotycznego. Ciśnienie to przewysza wytrzymałość betonu na rozciąganie co w efekcie prowadzi do powstawania spękań. Powstający żel w miarę wzrostu zawartości wody może się przemieszczać w betonie, wypełniając pory i powstałe spękania.

3. Metody badań występowania reakcji alkalia-krzemionka

Wśród najbardziej popularnych metod stosowanych do oceny reaktywności kruszyw z alkaliami,

zarówno wg norm amerykańskich ASTM jak i europejskich RILEM, wyróżnia się metody petrograficzne oraz metody chemiczne. Badanie reaktywności alkalia-kruszywo dokonywane jest poprzez:

- analizę petrograficzną kruszywa,
- analizę próbek zapraw i betonów w ultraszybkich testach laboratoryjnych,
- analizę próbek zapraw i betonów w testach długoterminowych.

3.1. Analiza petrograficzna kruszywa

Wśród metod petrograficznych, w amerykańskiej metodzie ASTM C 295 [2], do oceny reaktywności kruszyw krzemionkowych zastosowanie znalazły: mikroskopia optyczna, skaningowa mikroskopia elektronowa z dyspersją energii (EDS) i dyfrakcją rentgenowską (XRD), spektroskopia w podczerwieni, analiza termiczna. Analizy dokonuje się na próbce w formie rdzenia, przekroju lub kawałka kruszywa. Analiza uzyskanego obrazu umożliwia przede wszystkim oznaczenie jakościowe (mikroskopia optyczna) i ilościowe mineralów, wykrywanie pustek, określanie rozmiarów i kształtów ziaren (komputerowa analiza obrazu).

W odniesieniu do kruszyw krzemionkowych, wśród minerałów reaktywnych wymienić należy: opal, krystobalit, trydymit, obsydian, szkło krzemionkowe, rogowiec, chalcedon, kryptokrystaliczne skały wulkaniczne, tj. andezyt, riolit, kwarc metamorficzny w stanie naprężeń i mikrokryystaliczną krzemionkę [3].

Metody petrograficzne pozwalają na zidentyfikowanie form reaktywnych krzemionki, jednak jest to zadanie trudne ze względu na problemy w wydzieleniu poszczególnych form. Jest to więc jeden z powodów stosowania również metod dylatometrycznych w celu oceny reaktywności kruszywa i połączenia ich z metodami petrograficznymi. Choć badanie nie może dostarczyć informacji dotyczących zachowania kruszywa w obecności alkaliów z cementem, pozwala na wybranie odpowiedniej metody przyspieszonej, kolejnej z metod badania reaktywności kruszywa.

RILEM AAR1 [4] przewiduje badania mikroskopowe reaktywności próbek kruszyw, opierające się na: separacji cząstek i obserwacji ich przekroju (procedura dość niepewna, niewłaściwa do badania nieznanych lub złożonych kruszyw), technice punktowej (uważana jest za najbardziej dokładną z dostępnych metod), petrografii całej skały. W wyniku badań, kruszywa klasyfikuje się do jednej z trzech klas: I – kruszywa nie reaktywne, II – kruszywa potencjalnie reaktywne, III – kruszywa reaktywne.

3.2. Analiza próbek zapraw i betonów w ultraszybkich testach laboratoryjnych

a) metoda przyspieszona ASTM C 1260 [5]

W metodzie wykorzystuje się cechę charakterystyczną dla większości reakcji chemicznych – reakcja przebiega szybciej w wyższej temperaturze.

Beleczki zapraw o wymiarach 25x25x250 mm (w metodzie RILEM AAR-2 wymiary 40x40x160 mm) [4], współczynnik w/c równy około 0,5 przechowuje się w 1M roztworze NaOH w temperaturze 80°C. Zmiany długości próbek oznaczone w 4, 7, 11, 14 dniu odnosi się do pomiaru początkowego, dokonanego na próbkach przechowywanych przez 24 h w wodzie w temperaturze 80°C. W metodzie ultraszybkiej otrzymana różnica długości większa od 0,1%, a mniejsza od 0,25% wskazuje na kruszywo średnio reaktywne, ekspansja powyżej 0,25% na kruszywo bardzo reaktywne. Równocześnie ekspansja poniżej 0,1% wartości początkowej wskazuje na kruszywo nie reaktywne.

W przeciwieństwie do metody ASTM C 227 w metodzie ASTM 1260 wraz ze spadkiem wskaźnika w/c spada również stopień ekspansji (prawdopodobnie spada stopień migracji jonów alkalicznych w próbce). Stwierdzono również, że wysoka temperatura i stężenie NaOH powoduje spadek zawartości jonów wapnia w roztworze mieszczącym się w porach materiału przez co zwiększa się rozpuszczalność i dyfuzja krzemionki z roztworu na zewnątrz. Efekt ten skutkuje spadkiem obserwowanej ekspansji. Metoda ta może więc dawać błędne wyniki.

Według przeprowadzonych badań, metoda ASTM 1260 daje ok. 36% wyników fałszywie negatywnych [6]. Tak wysoką liczbę niepowodzeń można zmniejszyć poprzez zmniejszenie kryterium reaktywności z 0,1% do 0,06% przy pomiarach 14-dniowych i 0,13% dla pomiarów wydłużonych do 28 dni. Celowość wydłużenia czasu badań została potwierdzona przez niektórych badaczy reaktywności kruszyw [7].

b) metoda badania próbek zapraw w autoklawie

Metoda ta ukazywana jest jako najbardziej obiecująca dla określenia reakcji alkalia-krzemionka. Próbki zapraw wykonywane są zgodnie z metodą ASTM C 227 jednak przy współczynniku w/c wynoszącym 0,50 i zawartości alkaliów równych 3,50% Na₂O_e. Próbki umieszczane na 5 godzin w autoklawie przy ciśnieniu 0,17 MPa i temperaturze ok. 130°C podlegają pomiarom długości. Stwierdzono, że test ten jest bardziej wiarygodny od przyspieszonej metody ASTM C 1260. Proponowany limit ekspansji wynoszący 0,1% został uznany za dopuszczalny [8].

c) normy europejskie

Według europejskiej normy AAR-4 (metoda przyspieszona) i AAR-4 Alt. (metoda alternatywna) próbki betonu o rozmiarach (75±5)x(75±5)x(250±50) mm są przechowywane w temperaturze 60°C. W metodzie AAR-4 próbki przechowywane są w pojemnikach, nad lustrem wody, a w metodzie alternatywnej próbki zawijane się w wilgotną tkaninę bawełnianą i polietylen. Pomiarów stopnia ekspansji dokonuje się przez okres 20 lub 15 tygodni. Wyniki testu AAR-4 wykazujące ekspansję wyższą niż 0,03% wskazują na kruszywo reaktywne [9].

3.3. Analiza długoterminowa

a) metoda ASTM C227 [10]

W metodzie ASTM C 227 stosuje się cementy o zawartości alkaliów wynoszącej 0,60% Na₂O_e. Norma nie określa ściśle wartości współczynnika w/c. Beleczki (25x25x250 mm) po dobie od zarobienia przechowuje się w 38°C±2°C w specjalnych pojemnikach nad lustrem wody. Pomiarów długości ostudzonych do 23°C próbek dokonuje się po 14 dniach oraz 1, 2, 3, 4, 6, 9, 12 miesiącach, jeśli to konieczne również po każdym sześciu miesiącach od tego. Różnica długości początkowej próbki i zmierzonej po 12 miesiącach większa niż 0,1% pozwala twierdzić, że kruszywo jest reaktywne. Wynik poniżej 0,1% świadczy o braku reaktywności.

Badania przeprowadzane w wielu ośrodkach pozwoliły stwierdzić, że test ten nie pozwala przewidzieć reaktywności w przypadku wielu wolno reagujących kruszyw np. szarogłaz, argillit [5]. Równocześnie zastosowanie pojemników, do przechowywania próbek, wyposażonych w wojłoki związane jest z wymywaniem alkaliów z zapraw, co skutkuje zmniejszeniem stopnia ekspansji. Stąd uważa się, że należy zwiększyć zawartość alkaliów do 1,25%, a stosunek w/c nie powinien przekroczyć wartości 0,50.

b) metoda ASTM C 1293 badania próbek betonowych [11]

W metodzie tej próbki betonu o wymiarach 75x75x285 mm przechowywane są nad wodą, przy 100% wilgotności, w szczelnych pojemnikach przy temperaturze 38°C. Pomiarów długości próbek dokonuje się w 7, 28, 56 dniu oraz po 3, 6, 9, 12 miesiącu i jeśli to konieczne po każdych sześciu miesiącach od tego okresu. Ekspansja wynosząca po okresie roku 0,04% świadczy o potencjalnej reaktywności kruszywa. Zastosowanie tej metody jest istotne w przypadku, gdy badania petrograficzne nie dały przesłanek do stwierdzenia reaktywności kruszywa podczas gdy próby wykonane na zaprawach dały wynik potwier-

dzający reaktywność. Wadą metody jest niewątpliwie długi czas jej przeprowadzania.

Podsumowanie

W przedstawionych metodach badania potencjalnej reaktywności kruszyw krzemionkowych kluczową rolę odgrywają determinanty reakcji alkalia-krzemionka. Ze względu na fakt, iż reakcja alkalia-krzemionka ujawnia się po dłuższym okresie, zwiększenie parametrów takich jak: temperatura, ciśnienie, stężenie alkaliów, wilgotność w opisanych metodach badań pozwala na wnioskowanie o zachowaniu kruszywa w rzeczywistych budowlach.



environment
environment

LIDIA DĄBEK¹
EWA OZIMINA²
ANNA PICHETA-OŁĘŚ³

Kielce University of Technology
Faculty of Civil and Environmental Engineering
al. Tysiąclecia Państwa Polskiego 7
25-314 Kielce, Poland

¹ e-mail: ldabek@tu.kielce.pl,
² e-mail: ozimina@tu.kielce.pl,
³ e-mail: vika12@gazeta.pl

ASSESSING THE EFFECT OF IRON IONS ADSORBED ON ACTIVATED CARBON AND THE EFFICIENCY OF DECOMPOSITION OF ORGANIC IMPURITIES USING SELECTED OXIDIZING AGENTS

Abstract

This study analyzes the effect of Fe (II) ions adsorbed on activated carbon on the efficiency of phenol decomposition, using H_2O_2 , Fe_2^{+}/H_2O_2 (Fenton's reaction) and 1:1 HNO_3 solutions (in the third case, in the presence of microwaves), and, accordingly, their effect on the sorptive capacity of regenerated activated carbons. The chemical regeneration of the activated carbons using the Advanced Oxidation Process (AOP) method resulted in partial oxidation of the adsorbed organic substance. The presence of Fe(II) ions improved the efficiency of the regeneration process. The oxidation of the adsorbed phenol, however, caused a significant loss of mass of the activated carbon.

Keywords: activated carbon, sorption, regeneration, oxidation, heavy metals

1. Introduction

Removing toxic organic substances from wastewater is a difficult and complex problem and can be achieved by applying physical, chemical, electrochemical and biological methods. Wastewater from the chemical, petrochemical, coke and pharmaceutical industries is particularly difficult to treat, as it contains aromatic organic compounds such as phenol and phenol derivatives. Today, the Advanced Oxidation Process (AOP), which involves using H_2O_2 or Fenton's reaction (Fe^{2+}/H_2O_2), is becoming a more and more popular method of treating organic industrial waste [4, 5, 9]. In this case, hydroxyl radicals generated in the reaction environment are the oxidizing agent [4-9]. An alternative is applying the process of oxidation of the organic compounds previously adsorbed on activated carbon [4-9]. The literature on the subject, for example [4, 6, 8, 9], confirms that activated carbon, added to hydrogen peroxide or Fe^{2+}/H_2O_2 solutions and organic substances, not only plays

the role of a sorbent but also catalyzes the process of formation of hydroxyl radicals. Since the formation of hydroxyl radicals during a Fenton's reaction is directly related to the presence of Fe^{2+} ions, it is essential to determine whether the presence of this metal on the surface of activated carbon affects the effectiveness of the oxidation of the adsorbed organic substances. In this study, the problem was analyzed using the example of oxidation of phenol adsorbed on activated carbon.

2. Experiment

2.1. Isotherms of sorption of Fe(II) ions and phenol from aqueous solutions on virgin and regenerated activated carbons

0.5 g samples of different activated carbons were weighed into conical flasks and treated with 200 cm³ of solutions containing Fe(II) ions with concentrations ranging from 1.5 mg/dm³ to 40 mg/dm³ and phenol (Ph) with concentrations ranging from 50 mg/dm³ to 750 mg/dm³. The flasks were then shaken for three hours. The sorption isotherms were determined for

phenol, Fe^{2+} ions, and phenol and Fe^{2+} ions in the following order: F-300-Ph, F-300-Fe-Ph, F-300-Ph-Fe and F-300-(Fe/Ph).

2.2. Determination of the concentrations of Fe^{2+} ions and phenol

The metal concentration was determined through MERCK Spectroquant tests using a Spectroquant NOVA 60 spectrophotometer. The concentration of phenol was established using a gas chromatograph equipped with a Thermo Scientific MS Focus GC detector and a TRACE-TR-1MS column, operating at temperatures of 40–260°C.

2.3. Regeneration of activated carbons by oxidation of the adsorbed organic impurities

a. using hydrogen peroxide

Five-gram samples of different activated carbons, saturated with phenol and iron ions, were weighed into flasks and treated with 200 cm³ of a hydrogen peroxide solution with a concentration of 0.7 M/L and a pH of 8.1. The samples were then mixed for one hour. The hydrogen peroxide solution was decanted, and the activated carbons were rinsed first with acidified distilled water (1x100 cm³), then with distilled water (4x100 cm³), and, finally, dried at a temperature of 378 K.

b. using Fenton's reaction

Five-gram samples of the analyzed activated carbons, saturated with phenol and iron ions, were placed in 200 cm³ conical flasks and treated with 100 cm³ of distilled water. Then, FeSO_4 and H_2O_2 solutions (with a pH of 3–4) were added simultaneously, maintaining a weight ratio of 1:5 between Fe^{2+} and H_2O_2 . The samples were then shaken for three hours. Subsequently, the solution with Fenton's reagent was decanted, and the carbon was rinsed first with a basic solution (1x30 cm³) with a pH of ~8 to stop the oxidation reaction and then with distilled water (4x100 cm³) and, finally, dried at a temperature of 378 K until a solid mass formed.

c. using an HNO_3 solution in the presence of microwaves

The carbon samples were treated with a 1:1 HNO_3 solution (the proportion being 1g of regenerated activated carbon per 10 cm³ of the oxidizing solution) and then heated for 5 minutes using a microwave field with a frequency of 2450 MHz produced by a Plazmatronika UniClever microwave mineralizer at 80% of the generator's power. The solution above

the carbon was decanted three times. The regenerated activated carbons were rinsed with distilled water until a neutral reaction was reached. Then, they were dried at a temperature of 378 K until a solid mass formed.

2.4. Characteristics of the activated carbons

The porous structure was determined by conducting low-temperature adsorption of nitrogen (77 K). The isotherms of adsorption and desorption were established with the volumetric method by means of a Sorptomatic 1900 analyzer. The total content of the acidic groups was determined through a titration analysis with a 0.01M HCl solution by titrating the excess of the unreacted 0.01M NaOH, which was previously used for treating the carbon samples.

3. Discussion of results

In this study, we analyzed the sorption of phenol (Ph) on virgin F-300 activated carbon (F-300-Ph) and F-300 activated carbon with previously adsorbed Fe(II) ions (F-300-Fe-Ph), the sorption of Fe(II) ions on the carbon with previously adsorbed phenol (F-300-Ph-Fe) as well as the simultaneous sorption of phenol and iron ions (F-300-(Fe/Ph)). The activated carbon selected for the tests, F-300, is characterized by an extended porous structure (Table 1) and moderate surface acidity. The sorptive capacities of virgin F-300 carbon in relation to phenol and Fe(II) ions were 180 mg/g and 5.5 mg/g, respectively (Table 2). It was also found that the previously adsorbed Fe(II) ions did not reduce the sorption of phenol. The results indicate that iron ions were sorbed on active centres other than phenol, but they actively participated in the process. The findings correspond to the results presented in [1–3], which suggest that the sorption of metals takes place on acidic oxygen groups on the surface of the activated carbon, while the presence of basic functional groups contributes to the sorption of phenol. Moreover, the presence of metal improves the sorption of phenol as a result of donor-acceptor interactions. The sorption of the metal ions on the activated carbon with adsorbed phenol was lower, i.e. 5 mg/g for Fe(II). This indicates that, because of their size, the adsorbed particles of phenol cover the active centres capable of sorption of the metal ions or change the chemical character of the surface of the activated carbon. The sorption from the metal ion-phenol mixture, F-300-(Fe/Ph), is much lower; it is 4 mg/g and 110 mg/g for Fe(II) and phenol, respectively. This might be a result of the competition in the diffusion region as well as the occurrence of donor-acceptor interactions between phenol and iron ions in the solution.

Table 1. Characteristics of the virgin F-300 and regenerated carbons

Samples	Oxidation conditions	S [m ² /g]	V [cm ³ /g]	Surface acidity [mmol/g]	Mass loss [%]
F-300	-	965	0.57	0.57	-
F-300/HNO ₃	activated carbon/1:1 HNO ₃ /2450 MHz/80%/5 min	850	0.72	2.20	25
F-300/ H ₂ O ₂	activated carbon/ 0.7 M H ₂ O ₂ /L/60 min	960	0.68	1.60	12
F-300/Fe/ H ₂ O ₂	Fe : H ₂ O ₂ 1:5/60min	910	0.70	1.80	22

Table 2. Comparison of the sorptive capacity of the virgin activated carbon, F-300, in relation to iron ions and phenol from aqueous solutions, according to the order of sorbed substances

F-300 activated carbon-component sorbed as the first-component sorbed as the second (sorption from the mixture)	Sorptive capacity for iron ions, mg/g	Sorptive capacity for phenol, mg/g
F-300	-	180
F-300-Fe-Ph	5.5	170
F-300-Ph-Fe	5.0	180
F-300-(Fe/Ph)	6.0	110

Saturated with phenol and iron ions, the samples of activated carbons were then subjected to chemical regeneration using the following oxidizing agents: a 1:1 HNO₃ solution, in the presence of microwaves [3], a 0.7 M H₂O₂ solution with a pH of 8.1, which, as stated in Ref. [4], contributes to the formation of OH* radicals, and an Fe²⁺/H₂O₂ solution with a pH of 3-4 (Fenton's reaction), responsible for the formation of OH* radicals. It should be noted that the amount of oxidant in the reaction environment was selected in such a way as to ensure oxidation conditions according to stoichiometry.

First, it was vital to assess the influence of the oxidants on the F-300 activated carbon. The results in Table 1 show that the oxidants were responsible for the changes in the porous structure as well as the chemical properties of the sorbent surface. The greatest changes were due to the action of 1:1 nitric acid (V) on the activated carbon. At the boiling point of the solution exposed to microwaves, there was a substantial decrease in the surface area from 965 m²/g to 850 m²/g, and a simultaneous increase in the pore volume, which suggests destruction of the micropores and a rise in the volume of mesopores. The high acidity of the surface testifies to a considerable increase in acidic functional groups. The presence of hydrogen peroxide as well as

Fenton's reagent results in a significant increase in the surface acidity after oxidation, but the changes in the porous structure are negligible. It should be emphasized that in each case there was a considerable loss of mass of the activated carbon.

Applying analogous conditions of oxidation for carbons saturated with phenol and metal ions, i.e. Fe(II), resulted in partial oxidation of phenol. It was possible to reuse the activated carbons to remove the substance from an aqueous solution. The results in Table 3 indicate that:

- the partial oxidation of phenol, occurring after treating activated carbon with an H₂O₂ or an Fe₂+/H₂O₂ solution, was not dependent on the amount of adsorbed Fe(II) ions or the order of sorption; the partial oxidation allowed resorption of 100 mg/g of phenol; the sorption, however, was higher in the presence of Fe(II) ions adsorbed by the activated carbons; direct action of hydrogen peroxide did not lead to phenol oxidation;
- applying a 1:1 HNO₃ solution on carbons saturated with phenol and Fe(II) ions caused a considerable decrease in the sorptive capacity of the carbons in relation to phenol from 180 mg/g to 90 mg/g due to oxidation; the sorptive capacity of the carbons with regard to iron ions was higher for carbon saturated with phenol only (F-300-Ph) than for virgin carbon (F-300).

In studying the efficiency of oxidation of phenol adsorbed on the F-300 activated carbon, it was found that the oxidation was only partial under the predetermined conditions, maintaining the stoichiometric ratio of the adsorbed organic substance to the oxidant. This might be due to the fact that phenols adsorbed on activated carbons are prone to polymerization, which is likely to change the oxidation process. Moreover, the amount of oxidant required for the reaction may be higher than when the process takes place in a solution. Another reason for the partial oxidation of phenol might be the reaction of the oxidant with the carbon matrix, which results in a considerable loss of mass of the activated

carbon. The presence of metal on the surface of the activated carbon is also responsible for a greater loss of the sorbent mass.

Table 3. Assessing the sorptive capacity of the spent F-300 activated carbon according to the regeneration conditions and the order of sorbed substances

Regenerated activated carbon	Regenerating/oxidizing agent	Sorptive capacity of regenerated activated carbon, mg/g			
		Unary solutions		Mixture (Fe/Ph)	
		Fe	Ph	Fe	Ph
F-300	H ₂ O ₂	4	120	4	120
	Fe/H ₂ O ₂	6	110	6	100
	1:1 HNO ₃	6	80	6	90
F-300-Fe-Ph	H ₂ O ₂	2	110	2	120
	Fe/H ₂ O ₂	3	100	3	100
	1:1 HNO ₃	3	90	3	90
F-300-Ph-Fe	H ₂ O ₂	2	120	2	120
	Fe/H ₂ O ₂	2	110	2	100
	1:1 HNO ₃	3	90	3	90
F-300-(Fe/Ph)	H ₂ O ₂	2	120	2	120
	Fe/H ₂ O ₂	2	100	2	100
	1:1 HNO ₃	3	90	3	90

The results show that the chemical regeneration of the activated carbons saturated with phenol using such oxidants as H₂O₂ and Fe²⁺/H₂O₂ resulted in partial oxidation of the adsorbed organic substance. The presence of adsorbed Fe(II) ions increased the efficiency of the regeneration, and, in consequence, the sorptive capacities of the regenerated activated carbons. However, the oxidation of the adsorbed organic substance led to a considerable mass loss of the activated carbon.

The work reported herein has been undertaken as part of project NN205 1993 33 funded by the Ministry of Science and Higher Education. In the academic year 2011/2012, Anna Picheta-Oleś, who is a PhD student at the Kielce University of Technology, has been awarded a grant co-financed by the EU European Social Fund within the Programme for the Development of the Educational Potential of the Kielce University of Technology: Education for success, Agreement No UDA-POKL.04.01.01-00-175/08-03, Priority IV, Measure 4.1, Action 4.1.1.

References

- [1] Bansal R. Ch., Goyal M.: *Activated Carbon Adsorption*, 2005, CRC Press.
- [2] Biniak S., Pakuła M., Szymański S., Świątkowski A.: *Effect of activated carbon surface oxygen- and/or nitrogen containing groups on adsorption of copper (II) ions from aqueous solution*, Langmuir, 1999, 15, pp. 6117-6122.
- [3] Dąbek L.: *Regeneracja zużytych węgli aktywnych (Regeneration of spent activated carbons)*, Monografie, Studia, Rozprawy, Wydawnictwo Politechniki Świętokrzyskiej, M1, Kielce 2007.
- [4] Huang H.H., Lu M.C., Chen J.N., Lee C.T.: *Catalytic decomposition of hydrogen peroxide and 4-chlorophenol in the presence of modified activated carbons*, Chemosphere, 2003, 51, pp. 935-943.
- [5] Luis A., Lombraña J.I., Varona F., Menéndez A.: *Kinetic study and hydrogen peroxide consumption of phenolic compounds oxidation by Fenton's reagent*, Korean J. Chem. Eng., 2009, 26(1), pp. 48-56.
- [6] Richard S., Horng R.S., Tseng I.-Chin,: *Regeneration of granular activated carbon saturated with acetone and isopropyl alcohol via a recirculation process under H₂O₂/UV oxidation*, Journal of Hazardous Materials, 2008, 154, pp. 366-372.
- [7] Tekin H., Bilkay O., Ataberk S.S., Balta T.H., Ceribasi H., Sanin D., Filiz B., Dilek F.B., Yetis U.: *Use of Fenton oxidation to improve the biodegradability of a pharmaceutical wastewater*, Journal of Hazardous Materials, 2006, B136, pp. 258-265.
- [8] Toledo L.C., Silva A.C.B., Augusti R., Lago R.M.: *Application of Fenton's reagent to regenerate activated carbon saturated with organochloro compounds*, Chemosphere, 2003, 50, pp. 1049-1054.
- [9] Vidic R.D., Suidan M.T., Sorial G.A., Brenner R.C.: *Effect of molecular oxygen on adsorptive capacity and extraction efficiency of granular activated carbon for three ortho-substituted phenols*, Journal of Hazardous Materials, 1994, Vol. 38, pp. 373-388.

Lidia Dąbek
 Ewa Ozimina
 Anna Picheta-Oleś

Ocena wpływu zaadsorbowanych na węglu aktywnym jonów żelaza na skuteczność degradacji zanieczyszczeń organicznych wybranymi czynnikami utleniającymi

1. Wprowadzenie

Usuwanie ze ścieków toksycznych substancji organicznych to trudny i złożony problem wymagający stosowania różnorodnych metod fizycznych, chemicznych, elektrochemicznych oraz biologicznych. Szczególnie trudne jest oczyszczanie ścieków pochodzących z przemysłu chemicznego, petrochemicznego, koksowniczego oraz farmaceutycznego zawierających aromatyczne związki organiczne w tym fenol i jego pochodne. W odniesieniu do tych ścieków coraz częściej rozważa się możliwość wykorzystania reakcji utleniania zanieczyszczeń organicznych metodą AOP (Advanced Oxidation Process) z wykorzystaniem H_2O_2 lub reakcji Fentona (Fe^{2+}/H_2O_2) [4, 5, 9]. W tym przypadku czynnikiem utleniającym są generowane w środowisku reakcji rodniki hydroksylowe [4-9]. Rozważa się również możliwość prowadzenia procesu utlenienia związków organicznych po ich wcześniejszym zaadsorbowaniu na węglu aktywnym [4-9]. Jednocześnie jak wskazują dane literaturowe [4, 6, 8, 9] węgiel aktywny wprowadzony do roztworu nadtlenku wodoru jak i Fe^{2+}/H_2O_2 oraz substancje organiczne, nie tylko pełni rolę sorbentu ale również katalizuje proces powstawania rodników hydroksylowych. Z uwagi na to, że w reakcji Fentona powstawanie rodników hydroksylowych jest bezpośrednio związane z obecnością jonów Fe^{2+} powstaje pytanie, czy obecność tego metalu na powierzchni węgli aktywnych wpływa na efektywność utleniania zaadsorbowanych substancji organicznych. To zagadnienie jest przedmiotem prezentowanej pracy i jest analizowane na przykładzie utleniania fenolu zaadsorbowanego na węglu aktywnym.

2. Część doświadczalna

2.1. Izotermy sorpcji jonów Fe(II) oraz fenolu z roztworów wodnych na węglu aktywnym świeżym i węglach zregenerowanych

W kolbach stożkowych odważono po 0,5 g badanych węgli aktywnych. Naważki zadawano odpowiednio roztworami (o objętości 200 cm³) zawierającymi jony Fe(II) w zakresie stężeń od 1,5 mg/dm³ do 40 mg/dm³ oraz fenol (Ph) w zakresie stężeń od 50 mg/dm³ do 750 mg/dm³. Całość wytrząsano przez 3 godziny. Wyznaczono izotermy sorpcji fenolu F-300-Ph i z roztworów wodnych w odpowiedniej kolejności (F-300-Fe-Ph, F-300-Ph-Fe) i ich mieszaniny F-300-(Fe/Ph).

2.2. Oznaczanie stężenia jonów Fe^{2+} i fenolu

Stężenie metalu oznaczono z wykorzystaniem testów MERCK Spectroquant przy użyciu spektrofotometru Spectroquant NOVA 60. Stężenie fenolu oznaczano z wykorzystaniem chromatografu gazowego z detektorem MS Focus GC Thermo Scietific, z kolumną TRACE-TR-1MS, pracującego w zakresie temperatur 40-260°C.

2.3. Regeneracja węgli aktywnych poprzez utlenianie zaadsorbowanych zanieczyszczeń organicznych

a. nadtlenkiem wodoru

Naważki 5 g badanych węgli aktywnych po nasyceniu fenolem i jonami żelaza zadawano 200 cm³ roztworu nadtlenku wodoru o stężeniu 0,7 M/L o pH 8,1 i całość mieszano przez 1 godzinę. Następnie roztwór nadtlenku wodoru dekantowano, a węgle aktywne przemywano 1x100 cm³ zakwaszonej wody destylo-

wanej oraz $4 \times 100 \text{ cm}^3$ wody destylowanej i następnie suszono w temperaturze 378 K.

b. z wykorzystaniem reakcji Fentona

W kolbach stożkowych o pojemności 200 cm^3 odważono po 5 g każdego z badanych węgli aktywnych nasyconych fenolem i jonami żelaza, a następnie dodano po 100 cm^3 wody destylowanej, po czym wprowadzono jednocześnie roztwory FeSO_4 i H_2O_2 (pH roztworu wynosiło 3-4) zachowując stosunek wagowy $\text{Fe}^{2+} : \text{H}_2\text{O}_2$ jak 1:5 i całość wytrząsano przez 3 godziny. Następnie roztwór z odczynnikiem Fentona dekantowano, węgiel płytko 30 cm³ roztworem zasady o pH ~8 (w celu przerwania reakcji utlenienia) oraz wodą destylowaną ($4 \times 100 \text{ cm}^3$) i suszono w temperaturze 378 K do stałej masy.

c. w środowisku kwasu HNO_3 w obecności mikrofal

Naważkę węgla zadawano roztworem kwasu 1:1 HNO_3 (w proporcji 1 g regenerowanego węgla aktywnego: 10 cm^3 roztworu utleniającego) i ogrzewano przez 5 minut z wykorzystaniem pola mikrofal o częstotliwości 2450 MHz (wykorzystując mineralizator mikrofalowy UniClever firmy Plazmatronika przy wykorzystaniu 80% mocy generatora). Następnie roztwór znad węgla zlewano. Procedurę powtarzano trzykrotnie. Zregenerowane węgle aktywne płytko 30 cm³ wodą destylowaną do odczynu obojętnego, a następnie suszono w temperaturze 378 K do stałej masy.

2.4. Charakterystyka węgli aktywnych

Strukturę porowatą określono na podstawie badań niskotemperaturowej adsorpcji azotu (77 K). Izoterię adsorpcji i desorpcji wyznaczono metodą objętościową przy użyciu aparatu SORPTOMATIC 1900. Sumaryczną zawartość grup o charakterze kwasowym oznaczono w analizie miareczkowej roztworem 0,01M HCl odmiareczkowując nadmiar nieprereagowanego 0,01M NaOH, którym uprzednio zadano próbki badanych węgli.

3. Omówienie wyników

W pierwszym etapie badań przeprowadzono sorpcję fenolu (Ph) na świeżym węglu aktywnym F-300 (F-300-Ph), na węglu aktywnym F-300 z zaadsorbowanymi wcześniej jonami Fe(II) (F-300-Fe-Ph) oraz sorpcję jonów metalu Fe(II) na węglu z zaadsorbowanym wcześniej fenolem (F-300-Ph-Fe), jak również równoczesną sorpcję fenolu i jonów żelaza (F-300-(Fe/Ph)). Wybrany do badań węgiel aktywny F-300 charakteryzuje się rozwiniętą strukturą porowatą (tab. 1), umiarkowaną kwasowością powierzchni

ni. Wyznaczona zdolność sorpcyjna świeżego węgla F-300 względem fenolu wynosi 180 mg/g, względem jonów Fe(II) wynosi 5,5 mg/g (tab. 2). Jednocześnie stwierdzono, że zaadsorbowane wcześniej jony Fe(II) nie wpływają na zmniejszenie sorpcji fenolu. Wyniki te wskazują, że jony żelaza sorbują się na innych centrach aktywnych niż fenol, ale również aktywnie uczestniczą w tym procesie. Jest to zgodne z danymi literaturowymi [1-3] wskazującymi, że sorpcja metali zachodzi na kwasowych grupach tlenowych na powierzchni węgla aktywnego, natomiast sorpcji fenolu sprzyja obecność grup funkcyjnych o charakterze zasadowym. Jednocześnie obecność metalu dzięki interakcji donorowo-akceptorowej zwiększa sorpcję fenolu. Natomiast sorpcja jonów metalu na węglu aktywnym z zaadsorbowanym fenolem jest mniejsza i wynosi dla Fe(II) 5 mg/g. To wskazuje, że zaadsorbowane cząsteczki fenolu z uwagi na swoją wielkość zasłaniają centra aktywne zdolne do sorpcji jonów metali albo zmieniają charakter chemiczny powierzchni węgla aktywnego. Sorpcja z mieszaniny jon metalu-fenol F-300-(Fe/Ph)) jest zdecydowanie mniejsza i wynosi dla Fe(II) 4 mg/g, a dla fenolu 110 mg/g. Fakt ten można wyjaśnić wynikiem konkurencji w obszarze dyfuzyjnym, jak i występowaniem oddziaływań donorowo-akceptorowych fenol-jon żelaza w roztworze.

Następnie nasycone fenolem i jonami żelaza węgle aktywne poddano chemicznej regeneracji wykorzystując jako czynniki utleniające: roztwór 1:1 HNO_3 w obecności mikrofal [3]; roztwór 0,7 M H_2O_2 (o pH 8,1, co zgodnie z danymi literaturowymi [4] sprzyja powstawaniu rodników OH^*); roztwór $\text{Fe}^{2+}/\text{H}_2\text{O}_2$ o pH = 3-4 (reakcja Fentona), w którym na skutek reakcji powstają rodniki OH^* . Należy podkreślić, że ilość utleniacza w środowisku reakcji została tak dobrana, aby zapewnić warunki utlenienia zgodne ze stochiometrią.

W pierwszym etapie oceniono wpływ działania utleniaczy bezpośrednio na węgiel aktywny F-300. Przedstawione w tabeli 1 wyniki wskazują, że na skutek działania czynników utleniających obserwuje się zmiany w strukturze porowej jak i charakterze chemiczny powierzchni sorbentu. Przy czym zdecydowanie największe zmiany zachodzą na skutek działania na węgiel aktywny kwasem azotowym (V) 1:1. W temperaturze wrzenia roztworu w obecności mikrofal obserwuje się znaczne obniżenie powierzchni właściwej z $965 \text{ m}^2/\text{g}$ do $850 \text{ m}^2/\text{g}$, przy jednoczesnym wzroście objętości porów, co wskazuje na niszczenie mikroporów i wzrost objętości mezoporów. Jedno-

częśnie wysoka kwasowość powierzchni świadczy o zdecydowanym wzroście kwasowych grup funkcyjnych na powierzchni węgla aktywnego. Natomiast w efekcie działania zarówno nadtlenku wodoru jak i odczynnika Fentona obserwuje się znaczący wzrost kwasowości powierzchni po utlenieniu, podczas gdy zmiany struktury porowatej są nieznaczne. Należy jednak podkreślić, że we wszystkich przypadkach obserwuje się znaczący ubytek masy węgla aktywnego.

Zastosowanie analogicznych warunków utleniania w stosunku do węgli nasyconych fenolem i jonami metalu Fe(II) skutkuje częściowym utlenieniem fenolu i możliwością ponownego zastosowania węgli aktywnych do usuwania tej substancji z roztworu wodnego. Przedstawione w tabeli 3 wyniki badań wskazują, że:

- na skutek działania zarówno roztworu H_2O_2 jak i Fe_2^+/H_2O_2 na węgiel aktywny niezależnie od zaadsorbowanych jonów Fe(II) jak i kolejności sorpcji, następuje częściowe utlenienie zaadsorbowanego fenolu, co stwarza możliwość powtórnej sorpcji fenolu na poziomie 100 mg/g. Przy czym sorpcja ta jest wyższa w przypadku tych węgli aktywnych, na powierzchni których obecne były zaadsorbowane jony Fe(II). Należy zaznaczyć, że bezpośrednie działanie nadtlenku wodoru na fenol nie prowadzi do utlenienia tego związku.
- w efekcie działania roztworu 1:1 HNO_3 na węgle nasycone fenolem i jonami Fe(II) następuje znaczne zmniejszenie zdolności sorpcyjnych względem fenolu z poziomu 180 mg/g do 90 mg/g po utlenieniu. Natomiast zaobserwowano wzrost zdolności sorpcyjnej względem jonów żelaza w przypadku utlenienia węgla aktywnego nasyconego tylko fenolem (F-300-Ph), w porównaniu do węgla świeżego F-300.

Przedstawione wyniki badań dotyczące oceny skuteczności utleniania fenolu zaadsorbowanego na węglu aktywnym F-300 wskazują, że w zadanych warunkach, zapewniających stechiometryczny stosunek ilości zaadsorbowanej substancji organicznej i utleniacza, następuje tylko częściowe utlenienie tej ostatniej. Przyczyną tego może być fakt, że fenole zaadsorbowane na węglach aktywnych mają tendencję do polimeryzacji, co prawdopodobnie ma wpływ na inny przebieg reakcji utlenienia i być może wymaga większej ilości utleniacza niż w przypadku, gdy proces ten biegnie w roztworze. Z drugiej strony przyczyną częściowego utlenienia fenolu może być reakcja utleniacza z matrycą węglową, o czym świadczy duży ubytek masy

węgla aktywnego. Również i w tym przypadku obecność metalu na powierzchni węgla aktywnego skutkuje większym ubytkiem masy sorbentu.

Przedstawione wyniki badań wskazują, że chemiczna regeneracja węgli aktywnych nasyconych fenolem z wykorzystaniem utleniaczy takich jak H_2O_2 oraz Fe^{2+}/H_2O_2 skutkuje częściowym utlenieniem zaadsorbowanej substancji organicznej. Obecność zaadsorbowanych jonów Fe(II) zwiększa skuteczność tej regeneracji, a tym samym zwiększa zdolność sorpcyjną zregenerowanych węgli aktywnych. Niestety negatywnym skutkiem procesu utleniania zaadsorbowanej substancji organicznej jest znaczący ubytek masy węgla aktywnego.

Praca sfinansowana przez Ministerstwo Nauki i Szkolnictwa Wyższego w ramach projektu badawczego nr N N205 1993 33. Studentka studiów III stopnia Anna Picheta-Oleś w roku akademickim 2011/2012 otrzymuje stypendium naukowe współfinansowane ze środków Unii Europejskiej w ramach Europejskiego Funduszu Społecznego – projekt „Program Rozwojowy Potencjału Dydaktycznego Politechniki Świętokrzyskiej w Kielcach: kształcenie na miarę sukcesu”, Umowa UDA-POKL.04.01.01-00-175/08-03, Priorytet IV, Działanie 4.1, Podziałanie 4.1.1.

EDYTA GROBELSKA

Kielce University of Technology
Faculty of Civil and Environmental Engineering
al. Tysiąclecia Państwa Polskiego 7
25-314 Kielce, Poland
e-mail: edytagrobelksa@gmail.com

THE IMPACT OF MOISTURE AND CYCLIC FREEZING ON THE NON-FREEZING WATER OF MONO-IONIC BENTONITES

Abstract

In this study the effects of cyclic freezing and moisture content on unfreezable water content were investigated. Six monoionic forms of bentonite were used in experimental program. Samples were tested with Differential Scanning Calorimetry (DSC) method. The analysis of the results was done with Universal Analysis 2000 software and JETHRO program. Using statistical analysis as the tool it can be assumed, that the unfreezable water content of bentonite depends to some extent on the soil moisture content. The influence of cyclic freezing on unfreezable water content was not statistically significant.

Keywords: bentonite, freeze-thaw cycle, differential scanning calorimetry, unfrozen water, unfreezable water

1. Introduction

Bentonites belong to the group of cohesive soils, being composed primarily of montmorillonite. This mineral is formed as a result of weathering volcanic tuffs in the alkaline and highly basic environment [1]. Hydromicas and montmorillonite are two most common argillaceous mineral. At present, this mineral is undergoing hypergenic processes which result in its metamorphosis. In Poland pure montmorillonite rocks are rare [2]. Despite this fact, conducting research on these soils is of real use not only for scientific reasons, but also practical ones – to be applied in industry. Many Polish companies deal in importing bentonites from abroad, e.g. from the USA, Slovakia and Turkey. The demand for this raw material is systematically growing, especially in broadly understood environmental protection, construction industry and even medical sciences. On account of their special expansive qualities and high adsorption potential for water, bentonites are applied for building protective barriers used in waste dumping. They are also indispensable in removing toxic chemical compounds from the environment [4]. In recent years it has become popular to use bentonites to seal dikes. In building industry bentonites are also used to stabilize boreholes and deep ditches.

The properties of montmorillonite clays are due to their specific structure of 2:1 type. The elementary surfaces of adjacent packets are occupied by oxygen atoms, which results in a weak bond between the packets. Molecules of water and other polar liquids may easily get into spaces, weakening the operating intermolecular forces. This provides excellent conditions for ionic exchange in these soils [1]. The minerals from this group are highly hydrophylic (they manifest a high level of swelling and considerable moisture.)

The structure of bentonites may undergo modifications as a consequence of: moisture, cyclic freezing, the kind of exchangeable action the changes in the above mentioned parameters influence many engineering-geological properties of the soil. The impact of the changeable action on the non-freezing water (whose content depends on the temperature) is well examined [5]. The objective of this work is to define the impact of moisture and cyclic freezing on the non-freezing water, whose content does not depend on temperature. Water has a significant impact on concrete. According to Lebiediev [6] there are 5 states of water in the ground: vapour, bound water (tightly or loosely bound water), free water (capillary and gravitational), water in the solid state, water of crystallization and chemically bound water. The equilibrium freezing temperature for

the free water is steady and equals 273.15 K (0°C). For soil this temperature (T_0) depends mostly on moisture [5, 7, 8]. This temperature is an important parameter in the water-soil system, as above this temperature ice is absent from the system. Kozłowski concluded [5] that a certain part of water does not freeze at the T_0 temperature. It is only through further lowering of the system temperature that the next portions of water freeze. In the wet ground there is a fraction of water, which does not change its state of matter in a broad range of negative temperatures. It is the so called non-freezing water. Its content is usually defined analogously to moisture expressed in the percentage share of the mass of the skeleton (1):

$$u = \frac{m_u}{m_s} \quad (1)$$

with: m_u – the mass of the unfrozen water, m_s – the mass of the skeleton.

The change of the content of the non-freezing water in the soil depends closely on the temperature (Fig. 1).

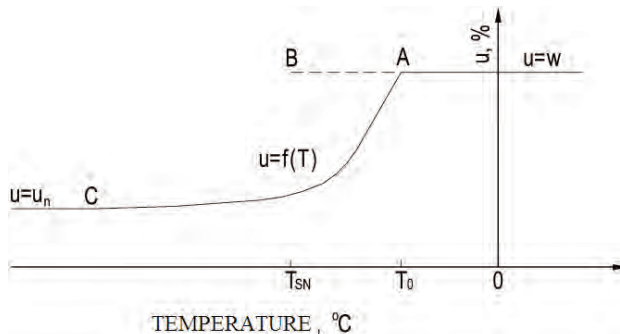


Fig. 1. The curve of the content of the unfrozen water in relation to temperature [5]

For temperatures higher than T_0 ice is not present in the system and the content of the unfrozen water u equals the total wetness w . During lowering the system temperature it is possible to overcool to the temperature of spontaneous nucleation T_{SN} (B of the diagram) in which crystallization begins. Next as a result of the emission of the latent heat there occurs a rapid increase of the temperature up to the value of T_0 (point A of the diagram). Further quasi-statistical cooling leads to a gradual change of the content of the unfrozen water on the way AC. During the warming up from the negative temperatures there occurs the increase of the content of the unfrozen water on the way CA. At the T_0 temperature the last ice crystals melt and the content of the unfrozen water equals w again [5].

In the water-soil system the following division of the non-freezing water can be assumed: unfrozen water

adsorbed on flat surfaces of crystallites, quasi-thin layer on top of ice and free water which does not freeze below 0°C [5].

In natural conditions a certain part of the unfrozen water does not freeze at all. This part is defined as the non-freezing water. The percentage share of the non-freezing water in the sample can be determined with equation (2). It is the difference between the total content of water in the sample and the content of ice [5].

$$u_n = w - \frac{100\Delta h}{Lm_s} \quad (2)$$

with: L – latent heat of the ice melting, Δh – the total heat effect of the ice melting, m_s – the mass of the skeleton.

The content of the non-freezing water in bentonites is to a certain degree connected with tightly bound water – so called hygroscopic water [2]. The properties of tightly bound water are similar to those of a solid. Moreover, this water has a considerable cohesiveness and resiliency. Its mean freezing temperature is -78°C and it depends on the mineral composition. It is estimated that with the temperature -70°C there is still 7% of the unfrozen water [9], according to the author it is only at -193.8°C that the water in soils freezes completely. The question of the impact of the cyclic freezing-thawing (CFT) on the non-freezing water appears an important issue to tackle. Engineering experiments prove that CFT has a negative impact on the subgrade soil [10]. Moreover Kozłowski's studies also proved [11] that this phenomenon modifies the specific surface area and the ion distribution parameters. Consequently, it may have an influence on the content of the non-freezing water. According to Anderson and Hoekstra [12], the inner-packet water of the bentonites migrates during freezing into the pore space and it is only there that the crystallization takes place. However, the results of the conducted SEM observations [11] revealed that the direction in which those microstructure's changes go is not so clear, which additionally hinders the proper defining of the impact of CFT on the non-freezing water. The diversity and ambiguity of the processes accompanying CFT was also discussed by Yong et al. [13] and Kumor [10].

This work attempts to answer the question: to what degree moisture and CFT affect the amount of the non-freezing water in mono-ionic bentonites. The basic experimental method to be used was the differential scanning calorimetry (DSC). The data obtained as a

result of this measurement will undergo an analysis developed by Kozłowski [5]. The obtained results underwent statistical analysis using the Stat-Crunch programme enabling data analysis in the network.

2. The characteristic of the examined soils

The research on the phase composition was conducted on the following samples:

- four mono-ionic forms of bentonite: B-Ca²⁺, B-Mg²⁺, B-Na⁺, B-K⁺;
- naturally sodium bentonite from Wyoming: B-Wy;
- naturally calcium bentonite from Texas: B-St.

Bentonite from Chmielnik, which is commonly regarded as a model bentonite [14] provided a base material for mono-ionic clays. It is practically a pure montmorillonite with 3-4% admixtures of volcanic glaze, quartz of pyroclastic origin, feldspars, biotites and chlorites [15]. The montmorillonite content on the basis of vapour sorption [16] accounted for 96% [5]. This value corresponds to the results of the analyses DTA, DTG and RTG published in the works of Heflik [15], and Grabowska-Olszewska [14]. The value of the total volume of the cation exchange C.E.C. amounts to 112.7 mval/100 g. In the sorption complex the calcium cation Ca²⁺ constitutes 87% and magnesium cation Mg²⁺ – 12% [14].

The mono-ionic forms of montmorillonite were obtained by repeated saturation of the fraction < 0.063 mm and eliminating the dissolved substances by diffusion. The pastes were then dried at room temperature until they achieved the required wetness and kept in a sealed container for app. Three weeks before the experiment. The detailed preparation of the samples is presented in Kozłowski's work [5]. The basic properties [5] are presented in Table 1. The values of the specific surface area were obtained by means of sorption test for vapour (WST) [16].

Table 1. The properties of mono-ionic forms of bentonites

Kind	Main cation	granulometric composition			Borders of consistency		Specific surface area [m ² /g]	
		[% C.E.C]	sand [%]	dust [%]	clay [%]	W _P [%]	W _I [%]	outer
B- Ca ²⁺	96	2	64	34	69.7	106.8	122	732
B- Mg ²⁺	96	5	61	34	75.8	105.9	122	732
B- Na ⁺	81	0	8	92	86.5	253.7	110	644
B- K ⁺	76	2	68	30	66.0	93.2	56	336

The basic properties of the bentonite from Wyoming and Texas are presented in Table 2.

Table 2. The properties of the bentonite from Wyoming and the bentonite from Texas

Origin	B- Wy	B- St
	USA, state of Wyoming, Crook county	USA, state of Texas, Gonzales county
Main cation	Na ⁺	Ca ²⁺
Volume of ionic exchange – C.E.C [mEq/100g]	76.4	84.4
Specific surface area (outer) by nitrogen sorption [m ² /g] [m ² /g]	31.82	83.79

3. The Methodology

The phase composition was studied by means of differential scanning calorimetry (DSC). It is the most suitable method presently available for studying the phase composition of water [5]. Calorimetric measurements were performed by means of DSC Q200 calorimeter produced by TA Instruments – a company recognized worldwide for high technology products. It has a built-in Tzero technology that provides the highest stability and repeatability of the base line combined with the highest sensitivity and resolution.

The calorimeter works according to the principle that the sample's temperature changes constantly within a certain assumed range. In a differential system the temperature changes occur simultaneously in the pan with the examined sample and in the empty reference pan. The possible thermal effects in the sample cause a delay or advance of the sample temperature against the temperature of the empty reference pan. In the graph showing the heat power output in relation to temperature $q(T)$ this fact is reflected as an appropriate peak (Fig. 2) The area under the graph of power in relation to time represents heat.

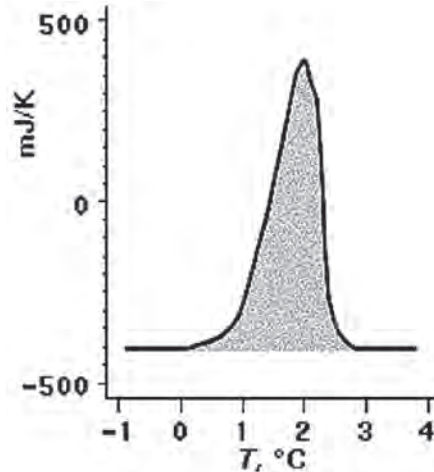


Fig. 2. An example of a registered DSC file

The identification of the file position (together with the temperature of the beginning T_p and the end (T_k) of the file) creates difficulties while analysing the DSC results. The phase transitions of pure crystallic substances give sharp peaks, whereas the ice melting in the water-soil system takes place in a wide range of temperatures and initially gives only insignificant thermal effects. The so called short-term noise resulting from the discontinuity of the calorimetric signal also makes the identification difficult. As a consequence of the noise, the rectilinear shape of the signal graph $q(T)$ in the range of the ice pre-melting temperatures merely approximates the real signal graph. Therefore, the base line approximation using the smallest squares method was performed. A set of signal values ranging from -20°C to -12°C was selected on the basis of the visual identification of the file beginning temperature for the received thermograms. It may be assumed that at the temperature of the phase change beginning the signal values start to move away from the approximating straight line. In consequence of the short-term noise, an accidental set of several adjacent signal values may appear above the base line [5]. Considering the presence of the short-term noise Kozłowski [5] developed an algorithm of searching the T_p temperature based on checking the succeeding signal values, starting from the maximum and moving towards the beginning of the file. The first encountered signal lower than the extrapolated value of the base line means the border of the straight line segment without the phase change and the preceding checked value constitutes the beginning of the file. Thus all the signal values within the file are higher than the values extrapolated by the base line equation. The method correctness was checked by using it to search the temperature of the beginning of the pure ice thawing file. An analogous procedure was used in order to find the end of the file temperature, but with the base line approximation within the range of +5°C to +9°C [5].

In order to define the heat of the phase change within new temperatures T_p i T_k , it is necessary to create between them "liquid" base line, taking into account the specific heat change of the sample ingredients. The „liquid” base line between T_p i T_k was constructed numerically according to Kozłowski's instructions [5]. Equation (3) describes the function of the file $h(T)$ corrected against the liquid base function:

$$h(T_i) = g(T_i) - \overline{g(T_i)} \quad (3)$$

assuming that:

$$\overline{g(T)} = a_s(T)T + b_s(T) \quad (4)$$

with: $\overline{g(T)}$ – quasi-linear equation describing the coordinates of points of the imagined base line within the range $[T_p; T_k]$; $a_s(T), b_s(T)$ – coefficients dependent on temperature.

The research method enabled:

- more precise defining of the characteristic temperatures of the T_p i T_k file,
- determining the liquid base line under the change file, connected with the change of the heat capacity of the sample in the course of the phase change,
- determining the function of the corrected file against the liquid base line $h(T)$,
- calculating the total heat effect of the phase change as the area under the file $h(T)$ and on this basis calculating the content of the non-freezing water u_n .

3.1. Research design

A sample of the soil paste in plastic state and weighing 5-12 mg was placed in the aluminium calorimetric pan with the diameter of 6 mm. In order to facilitate the heat flux, the samples were given a homogeneous form of a flat layer covering the bottom of the pan. The sealed pan with the sample was weighed with the accuracy of 10⁻⁶ g and kept in special containers. Directly before the examination the pan with the sample was weighed again to check the seal. After placing the pans in the socket A of the calorimeter (the empty reference pan was placed in socket B where it stayed all the time), the chamber of the calorimeter was locked and previously prepared research programme was started. The programme included 5 freeze-thaw cycles. The freezing was conducted at the rate of -2.5°C/min to the temperature of 90°C. After a 5-minute temperature stabilization at the level of 90°C there came the heating at the rate of 5°C/min to the temperature of 20°C. After a 30-minute stabilization the cycle was repeated 4 times. The examination of one sample in the calorimeter took over 8 hours. After that time the sample was taken out of the calorimeter and weighed again with the accuracy of 0.01 mg to check the seal. Then the calorimetric pan was pierced and dried at the temperature of 110°C in order to define the moisture.

5 samples of pastes were taken from each of the six kinds of bentonites and examined for the sake of this work. The final effect of the DSC was a period covering five full freeze-thaw cycles. Because of the overcooling (occurring during freezing) only the cycles of the sample thawing, marked with the succeeding

even numbers: 2, 4, 6, 8, 10, were examined in this work. The handling of data from the thermal analysis was done by means of the Universal Analysis 2000 software, which enabled separating single cycles from the graph and changing them into the digital form. The next step in the handling of the data was the work in the Jethro programme created by Kozłowski [5] in order to convert the change heat into the non-freezing water. The data prepared in such a form were later transformed to Excel and underwent statistical analysis by means of the StatCrunch software.

4. The research results

As it has been mentioned before, the content of the non-freezing water (u_n) may depend on many factors. They include e.g. the kind of the exchangeable cation, cyclic freezing, moisture. Comparing the mean values of the non-freezing water in different kinds of bentonites, it has been revealed that the impact of the mineral composition is significant (Table 3). It has been confirmed by the variance analysis (Table 4) and the presented diagram (Fig. 3).

Table 3. The general statistics of the non-freezing water

	B-Ca ²⁺	B-Mg ²⁺	B-Na ⁺	B-K ⁺	B-Wy	B-St
min u_n	29,57	26,80	28,48	15,79	21,79	25,79
max u_n	33,94	32,92	29,98	16,91	25,18	30,00
mean u_n	31,99	30,94	29,19	16,22	23,05	27,75

Table 4. Variance analysis – the impact of the cation on the non-freezing water

ANOVA table

Source	df	SS	MS	F-Stat	P-value
Treatments	5	3720.498	744.0996	420.54523	<0.0001
Error	119	210.55489	1.7693688		
Total	124	3931.053			

kation	Sample Var.	DF	Chi-Square Stat	P-value
Ca	1.7654786	24	42.371487	0.0234
K	0.1043142	19	1.9819698	<0.0001
Mg	4.045992	24	97.1038	<0.0001
Na	0.15678869	14	2.1950417	0.0003
St	1.9461882	19	36.977577	0.016
Wy	1.5750005	19	29.925009	0.1055

The value obtained in the test for the statistic F , smaller than 0.0001, is lower than the statistical significance 0.05. The null hypothesis should be rejected. That means that there are at least two groups in which the mean

values u_n significantly differ. The conducted chi-square test showed, that the impact of the mineral composition on the non-freezing water is significant on the level 0.05 in four out of five of the examined bentonites (Table 3). The significance of the mineral composition was also evaluated on the basis of the graph of the mean values u_n in the analysed groups (Fig. 3)

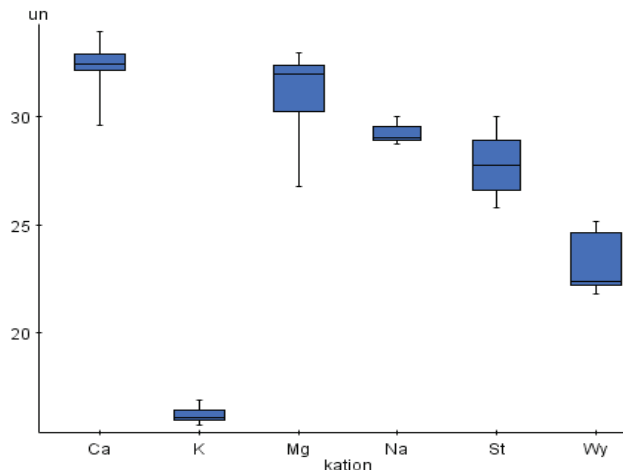


Fig 3. The content of the non-freezing water (%) in particular kinds of bentonite

4.1. The impact of the cyclic freezing on the non-freezing water in the bentonites

In order to evaluate the impact of the cyclic freezing, moisture, and the interaction of these factors on the non-freezing water (Table 5), the multiple regression analysis was conducted by means of the StatCrunch software. The non-freezing water was the dependent variable; whereas moisture, cycle (2, 4, 6, 8, 10) and the interaction of these factors were the independent variables. Figure 4 presents the distribution of the non-freezing water in different thawing cycles.

Table 5. The multi-factor variance analysis

Parameter estimates:

Variable	Estimate	Std. Err.	Tstat	P-value
Intercept	19.465328	5.4784517	3.5530708	0.0007
w	0.13835195	0.06567814	2.1065142	0.0393
CYKL	-0.17604262	0.8259077	-0.21315049	0.8319
CYKL * w	0.002066545	0.009901352	0.2087134	0.8354

Analysis of variance table for multiple regression model:

Source	DF	SS	MS	F-stat	P-value
Model	3	69.61051	23.203505	9.674584	<0.0001
Error	61	146.30228	2.398398		
Total	64	215.91278			

Summary of fit:

Root MSE: 1.5486761

R-squared: 0.3224

R-squared (adjusted): 0.2891

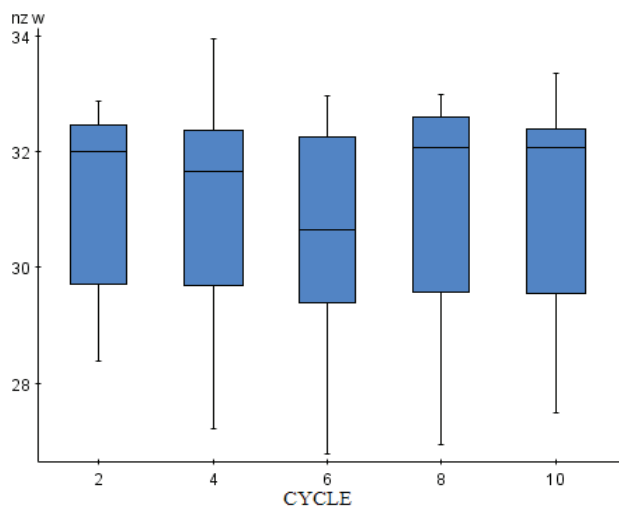


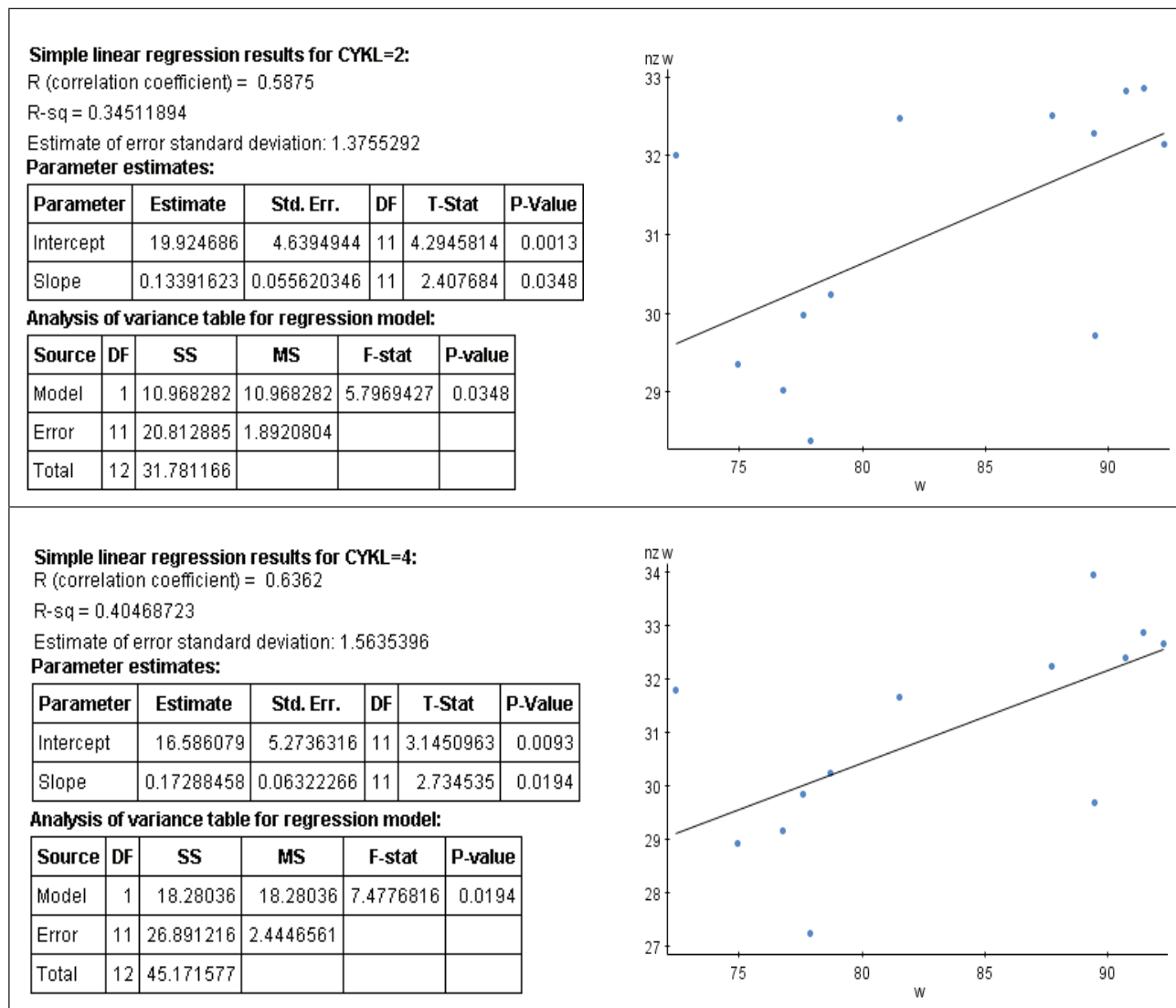
Fig. 4. The content of the non-freezing water (%) in different thawing cycles

The results of the regression analysis show that cyclic freezing does not have a significant impact on the content of the non-freezing water. The level of statistical significance is 0.83 and the null hypothesis is rejected at the level of 0.05. A similar result is visible in the impact on the non-freezing water of both moisture and cycle at the same time.

4.2. The impact of moisture on the non-freezing water in the bentonites

The impact of moisture on the non-freezing water showed considerable symptoms of the model significance (Table 5). The level of statistical significance was 0.039. Therefore a single-factor regression analysis was applied to evaluate the impact of moisture on the non-freezing water in different cycles (Table 6).

Table 6. The dependency of moisture on the non-freezing water in different cycles



Simple linear regression results for CYKL=6:

R (correlation coefficient) = 0.4564

R-sq = 0.20828068

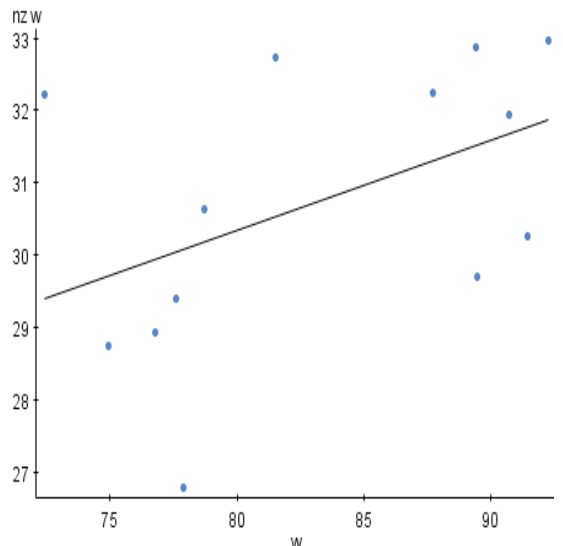
Estimate of error standard deviation: 1.8049862

Parameter estimates:

Parameter	Estimate	Std. Err.	DF	T-Stat	P-Value
Intercept	20.40678	6.0880017	11	3.3519669	0.0065
Slope	0.12415751	0.0729857	11	1.701121	0.117

Analysis of variance table for regression model:

Source	DF	SS	MS	F-stat	P-value
Model	1	9.427971	9.427971	2.8938127	0.117
Error	11	35.83773	3.2579753		
Total	12	45.2657			


Simple linear regression results for CYKL=8:

R (correlation coefficient) = 0.5758

R-sq = 0.33149105

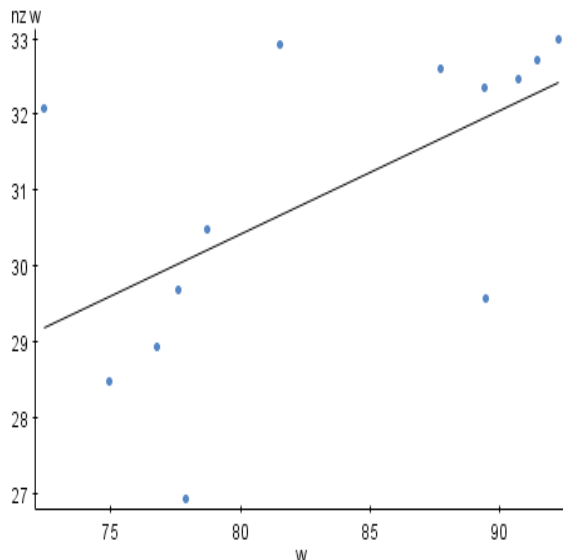
Estimate of error standard deviation: 1.7318155

Parameter estimates:

Parameter	Estimate	Std. Err.	DF	T-Stat	P-Value
Intercept	17.341028	5.8412056	11	2.9687414	0.0128
Slope	0.16354759	0.070026994	11	2.3354933	0.0395

Analysis of variance table for regression model:

Source	DF	SS	MS	F-stat	P-value
Model	1	16.35914	16.35914	5.4545293	0.0395
Error	11	32.99103	2.9991846		
Total	12	49.35017			


Simple linear regression results for CYKL=10:

R (correlation coefficient) = 0.5973

R-sq = 0.35671118

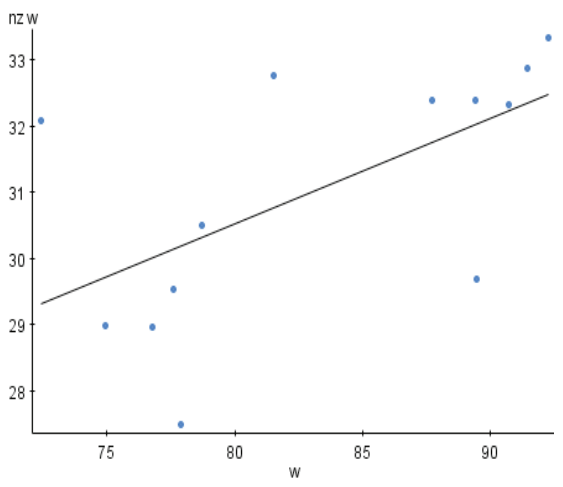
Estimate of error standard deviation: 1.5946461

Parameter estimates:

Parameter	Estimate	Std. Err.	DF	T-Stat	P-Value
Intercept	17.786785	5.37855	11	3.3069851	0.007
Slope	0.15925017	0.06448047	11	2.4697428	0.0311

Analysis of variance table for regression model:

Source	DF	SS	MS	F-stat	P-value
Model	1	15.510723	15.510723	6.099629	0.0311
Error	11	27.971857	2.5428963		
Total	12	43.482582			



In four out of five of the thawing cycles there have been noted considerable symptoms of the moisture effect on the non-freezing water. In each cycle the content of the non-freezing water increases with the rise of moisture.

5. Conclusions

1. Cyclic freezing does not have a practical effect on the content of the non-freezing water. It corresponds to the water adsorbed on flat areas of clay particles and most probably in the process of cyclic thawing the change of this area does not occur.
2. One may observe a certain insignificant impact of the total water content on the content of the non-freezing water. This fact could be possibly explained by the contribution of the quasi-liquid water layer formed on the ice crystals, to the total non-freezing water (and the more ice in the sample, the more water of this kind).
3. It is expected that the cyclic freezing will have effect on the form of the non-freezing water function, whose value depends on the pores distribution. This, however, requires completely new calculations.

This investigation was founded in part by the European Union within the framework of the European Social Fund project "Enhancing Educational Potential of Kielce University of Technology – Educating for Success" Operational Programme Human Capital, Agreement No UDA-POKL.04.01.01-00-175/08-00.

References

- [1] Grabowska-Olszewska B.: *Wpływ własności sorpcyjnych wybranych typów gruntów spoistych na ich hydrofilność.* Biuletyn Geol. UW, 1968, 10.
- [2] Grabowska-Olszewska B., Sergiejew J.M. (red.): *Gruntoznawstwo.* Wydawnictwo Geologiczne, Warszawa 1977.
- [3] Montes G., Duplay J., Martinez L., Mendoza C.: *Swelling-shrinkage kinetics of MX80 bentonite.* Applied Clay Science, 2003, 22, pp. 279-293.
- [4] Bergaya F., Lagaly G.: *Surface modification of clay minerals.* Applied Clay Science, 2001, 19, pp. 1-30.
- [5] Kozłowski T.: *Skład fazowy wody w gruntach spoistych poniżej 0°C.* Wydawnictwo Politechniki Świętokrzyskiej, Monografie Studia Rozprawy 6, 1997.
- [6] Liebiediew A.F.: *Gleby i wody gruntowe.* Moskwa 1936.
- [7] Low P.F.: *Some thermodynamic relationships for soils at or below the freezing point.* Water Resour. Res., 4.
- [8] Kozłowski T.: *Badania obniżenia punktu zamarzania wody w wybranych gruntach modelowych.* Archiwum Hydrotechniki PAN, XXXVII, s. 1-2.
- [9] Litwinowa T.A.: *Wpływ powierzchni ultraporowatości wiecznej zmarzliny na wodę niezamarzniętą.* Moskwa 1961.
- [10] Kumor M.K.: *Zmiana mikrostruktury ilów monomineralnych i ilu plioceńskiego pod wpływem cyklicznego przemrażania i odmrażania.* ATR w Bydgoszczy. Rozprawy 34, Bydgoszcz 1989.
- [11] Kozłowski T., Grobelska E., Walaszczyk Ł.: *Wpływ cyklicznego zamrażania na parametry mikrostruktury monojonowych bentonitów.* Zeszyty Naukowe Politechniki Zielonogórskiej, 2010, 19, s. 15-30.
- [12] Anderson D.M., Hoekstra P.: *Migration of interlamellar water during freezing and thawing of Wyoming bentonite.* Soil Sc. Soc. Am. Proc., 35.
- [13] Yong R.N. et al.: *Alternation of soil behavior after cyclic freezing and thawing.* Proc 4th Int. Sym. Ground freezing, Sapporo, Vol. 1, A.A. Balkema, Rotterdam 1985.
- [14] Grabowska-Olszewska B.: *Wpływ wilgotności sorpcyjnych wybranych typów gruntów spoistych na ich hydrofilność.* Biul. Geol. UW, 1968, 10.
- [15] Heftlik W.: *Petrography of volcanic Glass in bentonitic clays from Ciecierze near Chmielnik.* Kwart. Geol., 1959, 3, pp. 778-789.
- [16] Stępkowska E.T.: *Test sorpcyjny i możliwości jego stosowania w różnych badaniach.* Archiwum Hydrotechniki, t. XXIV, z. 3, s. 411-420.

Edyta Grobelska

Wpływ wilgotności i cyklicznego zamrażania na wodę niezamarzającą monojonowych bentonitów

1. Wprowadzenie

Bentonity należą do gruntów spoistych, zbudowanych głównie z montmorillonitu [1]. Jest to szeroko rozpowszechniony w przyrodzie minerał ilasty o unikalnych właściwościach: duże pęcznienie, wysoka wilgotność, dobre właściwości adsorpcyjne [2]. Głównym z czynników decydującym o tym jest specyficzna struktura bentonitów typu 2:1. Cechą charakterystyczną jest to, że powierzchnie elementarne sąsiadujących pakietów obsadzane są przez atomy tlenu co przyczynia się do słabej więzi między pakietami. W przestrzeniu łatwo mogą wchodzić cząsteczki wody i innych polarnych cieczy osłabiając działające siły międzymiążdżeczkowe. Stwarza to doskonałe warunki do wymiany jonowej w tych gruntach [1]. Szerokie spektrum zastosowań bentonitów wzmagających popyt na ten surowiec z każdym rokiem, szczególnie w szeroko rozumianej ochronie środowiska, budownictwie, a nawet medycynie [3, 4]. Istnieje jednak szereg czynników mogących modyfikować struktury bentonitów, jednocześnie warunkując zmiany w ich właściwościach np.: wilgotność, cykliczne zamrażanie, rodzaj kationu wymennego. Wpływ kationu wymennego na wodę niezamarzniętą (której zawartość zależy od temperatury) jest dobrze poznany [5]. Jako cel niniejszej pracy obrano określenie wpływu wilgotności i cyklicznego zamrażania na wodę niezamarzającą, której zawartość nie zależy od temperatury.

Istnieje wiele odmian wody w gruncie [6], które z kolei stanowią czynnik silnie oddziałujący na bentonity. Jak wiadomo temperatura zamarzania równowagowego wody wolnej (przy stałych warunkach ciśnienia) jest stała i wynosi 273,15 K (0°C). W przypadku gruntu wartość tej temperatury (T_0) zależy przede wszystkim od wilgotności [5, 7, 8]. Temperatura ta stanowi ważny parametr w systemie woda-grunt, jako temperatura powyżej której lód jest nieobecny w układzie. Kozłowski [5] stwierdził, iż pewna część wody nie zamarza w temperaturze T_0 . Dopiero dalsze obniżanie temperatury układu prowadzi do zamarzania kolejnych porcji wody. W wilgotnym gruncie istnieje frakcja wody, która nie zmienia stanu skupienia w szerokim zakresie temperatur ujemnych. Jest

to tzw. woda niezamarznięta. Jej zawartość określana jest zwykle analogicznie do wilgotności w procentach masy szkieletu (1). Zmiana zawartości wody niezamarzniętej w gruncie zależy ściśle od temperatury (rys. 1). W warunkach naturalnych pewna część wody niezamarzniętej w ogóle nie ulega zamarzaniu. Ta część wody określana jest jako woda niezamarzająca. Procentową zawartość wody niezamarzającej w próbce można wyznaczyć ze wzoru (2). Jest to różnica między całkowitą zawartością wody w próbce i zawartością lodu [5].

Zawartość wody niezamarzającej w bentonitach ma w pewnym stopniu związek z wodą silnie związaną tzw. higroskopijną [2]. Temperatura jej zamarzania wynosi średnio -78°C, przy czym jest zależna od składu mineralnego. Szacuje się, iż w temperaturze -70°C istnieje jeszcze 7% wody niezamarzniętej, według autorki pracy [9] dopiero przy temperaturze -193,8°C woda w gruntach całkowicie zamarza. Istotnym wydaje się tu podjęcie kwestii cyklicznego zamrażania – odmrażania (CZO) na wodę niezamarzającą. Doświadczenia inżynierskie przekonują nas o ujemnych skutkach CZO dla podłożu gruntowego [10]. Dodatkowo w pracy Kozłowskiego i in. [11] udowodniono, iż zjawisko to modyfikuje powierzchnię właściwą i parametry dystrybucji porów. Co za tym idzie, może mieć wpływ na zawartość wody niezamarzającej. Według Andersona i Hoekstry [12], woda międzypakietowa bentonitów migruje w trakcie zamarzania do przestrzeni porowej i dopiero tam odbywa się krystalizacja. Jednakże wyniki przeprowadzonych obserwacji SEM [11] wykazały, że kierunek zmian mikrostruktury nie jest jednoznaczny, co dodatkowo utrudnia właściwe określenie wpływu CZO na wodę niezamarzającą. O wielorakości i niejednoznaczności procesów towarzyszących CZO pisali również Yong et al. [13] oraz Kumor [10].

Niniejsza praca jest próbą odpowiedzi na pytanie: w jakim stopniu wilgotność i CZO wpływa na zmianę ilości wody niezamarzającej w bentonitach monojonowych? Jako podstawową metodę eksperymentalną wykorzystano kalorymetrię skaningową DSC. Dane uzyskiwane z każdego pomiaru zostaną poddane ana-

lizie opracowanej przez Kozłowskiego [5]. Uzyskane wyniki zostały poddane analizie statystycznej z użyciem programu StatCrunch umożliwiającego analizy danych w sieci.

2. Ogólna charakterystyka badanych gruntów

Badania składu fazowego prowadzono na próbkach:

- czterech monojonowych form bentonitów: B-Ca²⁺, B-Mg²⁺, B-Na⁺, B-K⁺;
- naturalnie sodowego bentonitu z Wyoming: B-Wy;
- naturalnie wapniowego bentonitu z Texasu: B-St.

Materiał wyjściowy dla czterech form bentonitów stanowił monomineralny bentonit z Chmielnika [15]. Szczegółową preparatykę próbek monojonowych można znaleźć w pracy Kozłowskiego [5]. Podstawowe właściwości zostały przedstawione w tabeli 1.

3. Metodyka badań

Badania składu fazowego prowadzono z wykorzystaniem różnicowej kalorymetri skaningowej (DSC) przy udziale aparatu TA typu DSC Q200. Jest to metoda najbardziej odpowiednia dla potrzeb badań składu fazowego wody spośród obecnie istniejących [5]. Metoda pozwala na szczegółowe określenie tych zmian wykorzystując do badania jedną próbki. Efekty termiczne objawiają się wystąpieniem odpowiedniego piku (rys. 2) (wraz z temperaturą początku (T_p) i końca piku (T_k)). Czyste substancje krystaliczne dają ostre piki co umożliwia określenie powyższych temperatur. Problem z ich identyfikacją pojawia się w przypadku topnienia lodu w systemie wodno-gruntowym, które zachodzi w szerokim zakresie temperatur i początkowo daje nieznaczne efekty termiczne. Identyfikację utrudnia również pojawienie się tzw. szumu krótkookresowego będącego skutkiem nieni ciągłości sygnału kalorymetrycznego. Problemy te zostały rozwiązane dzięki algorytmom stworzonym przez Kozłowskiego [5]. Ich wykorzystanie w niniejszej pracy pozwoliło na:

- bardziej precyzyjne określenie charakterystycznych temperatur piku T_p i T_k ;
- wyznaczenie płynnej linii bazy pod pikiem przemiany związanej ze zmianą pojemności cieplnej próbki w toku przemiany fazowej;
- wyznaczenie funkcji piku skorygowanego względem płynnej linii bazy $h(T)$;
- obliczenie całkowitego efektu cieplnego przemiany fazowej jako pola pod pikiem $h(T)$ oraz na jego podstawie obliczenie zawartości wody niezamarzającej u_n .

3.1. Procedura badawcza

Przed rozpoczęciem badania w aparacie DSC dokonano odpowiedniej preparatyki próbek. Grunty w stanie plastycznym o masie rzedu 5-12 mg umieszczano w aluminiowym naczyniu kalorymetrycznym jednocześnie nadając im formę płaskiej warstewki dla ułatwienia przepływu ciepła. Następnie hermetycznie zamykano naczynie z próbką i ważyono z dokładnością 10^{-6} g. Gotowe próbki umieszczano w komorze kalorymetru i załączano program badawczy. Obejmował on 5 cykli zamrażanie-odmrażanie. Zamrażanie przeprowadzono z prędkością $-2,5^{\circ}\text{C}/\text{min}$ do temperatury 90°C . Po 5-minutowej stabilizacji temperatury na poziomie 90°C następowało ogrzewanie z prędkością $5^{\circ}\text{C}/\text{min}$ do temperatury 20°C . Po 30-minutowej stabilizacji następowało czterokrotne powtarzanie cyklu. Badanie jednej próbki w kalorymetrze trwało ponad 8 godzin. Po tym czasie próbkę wyjmowano z kalorymetru i ponownie ważyono z dokładnością 0,01 mg dla sprawdzenia hermetyczności. Następnie naczynie kalorymetryczne przekłuwano i suszono w temperaturze 110°C w celu określenia wilgotności.

Efektem końcowym pracy DSC był wykres obejmujący 5 pełnych cykli zamrożenie-odmrożenie. Ze względu na zjawisko przechłodzenia (występujące podczas zamrażania) w pracy interpretowano jedynie cykle rozmrażania próbki, kolejno oznaczone numerami parzystymi: 2, 4, 6, 8, 10. Obróbka danych z analizy termicznej została wykonana przy użyciu oprogramowania Universal Analysis 2000, dzięki któremu wyodrębniano z wykresu pojedyncze cykle i zamieniano je na postać cyfrową. Kolejnym krokiem w obróbce danych była praca w programie Jethro stworzonym przez Kozłowskiego [5] dla celów przeliczenia ciepła przemiany na wodę niezamarzającą. Tak przygotowane dane były przepisywane do exela i dalej poddawane analizie statystycznej przy użyciu oprogramowania StatCrunch.

4. Wyniki badań

Analiza wariancji (ANOVA) i test chi-kwadrat wykazał znaczący wpływ kationu wymiennego na zawartość wody niezamarzającej w poszczególnych rodzajach bentonitów. Test chi-kwadrat wykazał, że wpływ składu mineralnego na wodę niezamarzającą jest istotny na poziomie 0,05 w czterech z pięciu badanych bentonitów (tab. 3).

Dla oceny wpływu cyklicznego zamrażania, wilgotności i współdziałania tych czynników na zawartość wody niezamarzającej posłużono się analizą regresji wykonaną przy użyciu oprogramowania StatCrunch.

4.1. Wpływ cyklicznego zamrażania na wodę niezamarzającą w bentonitach

Wyniki analizy regresji (tab. 4) wskazują, iż cykliczne zamrażanie nie wpływa istotnie na zawartość wody niezamarzającej. Poziom istotności wynosi 0,83. Podobny skutek widoczny jest we wpływie jednocześnie wilgotności i cyklu na wodę niezamarzającą.

4.2. Wpływ wilgotności na wodę niezamarzającą w bentonitach

Wpływ wilgotności na wodę niezamarzającą wykazał znaczne oznaki istotności modelu (tab. 5). Poziom istotności wyniósł 0,039. Posłużono się więc jednocyklową analizą regresji dla oceny wpływu wilgotności na wodę niezamarzającą w poszczególnych cyklach (tab. 6).

Zaobserwowano znaczne oznaki efektu wilgotność na wodę niezamarzającą w przypadku czterech z pięciu powyższych cykli rozmrażania. W każdym z cykli zawartość wody niezamarzniętej wzrasta razem z wilgotnością.

5. Wnioski

1. Cykliczne zamrażanie praktycznie nie wpływa na zawartość wody niezamarzającej. Odpowiada ona wodzie adsorbowanej na płaskich powierzchniach

częstek ilastycznych i najprawdopodobniej w procesie cyklicznego zamrażania nie dochodzi do zmian tej powierzchni.

2. Obserwuje się pewien nieznaczny wpływ wilgotności całkowitej na zawartość wody niezamarzającej. Możliwe wyjaśnienie tego faktu to wkład quasi-ciekłej warstewki wody na kryształkach lodu do całosci wody niezamarzniętej (a im więcej lodu w próbce, tym wiecej tego rodzaju wody).
3. Oczekuje się, że cykliczne zamarzanie wpłynie jednak na postać funkcji wody niezamarzniętej, której zawartość zależy od rozkładu porów. Wy-maga to jednak całkiem innych obliczeń.

Informuję, iż pobieram stypendium współfinansowane przez Unię Europejską w ramach Europejskiego Funduszu Społecznego projekt pt. „Program Rozwojowy Potencjału Dydaktycznego Politechniki Świętokrzyskiej w Kielcach-kształcenie na miarę sukcesu” Program Operacyjny Kapitał Ludzki, Umowa nr UDA-POKL.04.01.01-00-175/08-00.

ŁUKASZ J. ORMAN

Kielce University of Technology,
Faculty of Civil and Environmental Engineering
al. Tysiąclecia Państwa Polskiego 7
25-314 Kielce, Poland

e-mail: orman@tu.kielce.pl

MEASUREMENTS OF BOILING HEAT TRANSFER ON A SINGLE FIN

Abstract

Heat exchangers are part of mechanical devices. It is often important to determine the heat transfer characteristics of such exchangers to enable their proper design and operation. The article presents a combination of modern measuring techniques based on infrared technology and visualisation studies of boiling heat transfer on a fin – a basic heat exchanging element. The results obtained for distilled water are compared with a selected model of boiling from literature.

Keywords: boiling, heat transfer

1. Introduction

Boiling is a highly effective mode of heat transfer, which enables to dissipate significant amounts of heat – up to 10^6 W/m² and more. Consequently, attention is now paid to research into boiling due to a need to find efficient ways of cooling electronic or mechanical devices. It is also possible to produce smaller and more effective heat exchangers for refrigeration industry if boiling on specially prepared surfaces is applied.

Measurements of boiling heat transfer are almost always conducted on isothermal surfaces. Only a few works deal with boiling on non – isothermal surfaces, which are most often encountered in practical applications. Thus, it is necessary to carry out tests on a non – isothermal surface of a fin to determine a true nature of heat transfer in heat exchangers working with a change of phase of a coolant.

Boiling heat transfer is traditionally described with a boiling curve, which is a dependence of heat transfer coefficient or heat flux on wall superheat. The superheat is defined as a difference between saturation temperature of the liquid and surface temperature.

If the temperature of the heater surface is elevated over the boiling temperature of the fluid, at first no vapour bubbles are present and heat is transferred in the natural convection mode. Then, when the liquid is slightly superheated and superheat is high enough – ca. 2 to 6°C for water [2], boiling begins and vapour bubbles get created on the surface. It is a nucleate

boiling regime. Here, a sudden rise in dissipated heat is observed and heat transfer is more and more intense as the temperature of the surface is increased further. A rise in heat flux is linked with more vapour being produced and, consequently, neighbouring bubbles join together to finally produce a vapour film which insulates the surface from the liquid. It leads to a decrease in dissipated heat flux. A new unfavourable mode of heat transfer occurs – film boiling. Any further rise in heat flux is attributed mainly to radiation heat transfer [1]. From the practical point of view the most interesting mode of heat transfer is nucleate boiling, since it offers high heat dissipation rate at small temperature differences.

2. Experimental set – up

Generally, for many years a common technique to measure boiling heat transfer has been the use of experimental stands whose electric heater increased (or decreased) the measured temperature of the surface several times to determine points on the boiling curve. The temperature at every point of the surface has had to be the same (an isothermal surface), however, modern engineering devices are usually non – isothermal and research needs to be performed on finned surfaces, which is the focus of this paper.

The presented technique has been adopted from Orzechowski [5] and used to perform measurements on a single fin. The principal element of the experimental set – up is a vertical fin (Fig. 1). It is part

of one side of a vessel, in which liquid (in the present project distilled water) is boiled. On the inside the fin is in contact with the liquid and on the other side with air – this side is observed with an infrared camera. Heat is supplied to the base of this fin by an electric heater. Consequently, there is a temperature gradient along the fin. Measurements of temperature distribution have been conducted with a long-wave (8-14 μm) infrared camera equipped with a detector of 384 x 288 pixels whose thermal resolution is 0,08 K.

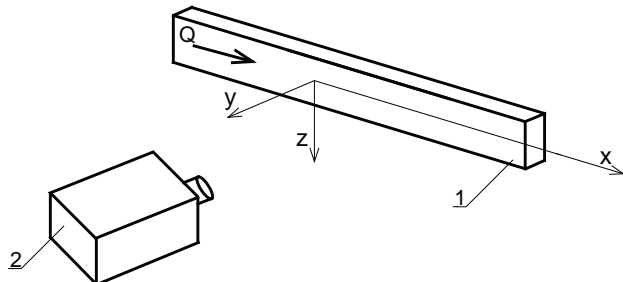


Fig. 1. Schematic of the measuring unit:
1 – fin, 2 – infrared camera [4]

Based on the temperature distribution along the fin and its numerical differentiation, assuming that boiling heat transfer coefficient depends exponentially on superheat, local values of the heat transfer coefficient are determined using a method presented by Orzechowski [5] and described below.

The formula for temperature distribution in the fin is:

$$\frac{d^2\theta}{dx^2} = m^2 \theta^{n+1} \quad (1)$$

which was analysed by Ünal in [7].

Parameter m^2 is defined as:

$$m^2 = \frac{aP}{\lambda F} \quad (2)$$

P and F stand for the circumference and area of the fin, respectively, while λ is the thermal conductivity of the fin's material. θ is a difference between surface temperature and saturation temperature of the liquid. Constants a and n are determined experimentally, which leads to the formula for heat transfer coefficient, according to the equation:

$$\alpha = a \theta^n \quad (3)$$

Differentiation of (1) leads to the relation for superheat gradient along the fin, which in logarithmic coordinates takes the form of:

$$\ln\left(\frac{d\theta}{dx}\right)^2 = \ln\left(\frac{2m^2}{n+2}\right) + (n+2)\ln\theta \quad (4)$$

For fins whose length is considerable no heat transfer at the tip can be assumed. In this case integration contact C is 0, as considered in (4).

From (3) the presented technique enables to determine the boiling curve as a function of local values of heat transfer coefficient and superheat based on the temperature distribution along the fin.

Figure 2 presents the temperature distribution on the smooth fin from Figure 1. It can be readily noticed that boiling heat transfer is very effective in cooling the element – temperature drops very close from the base of the fin and reaches the saturation temperature.

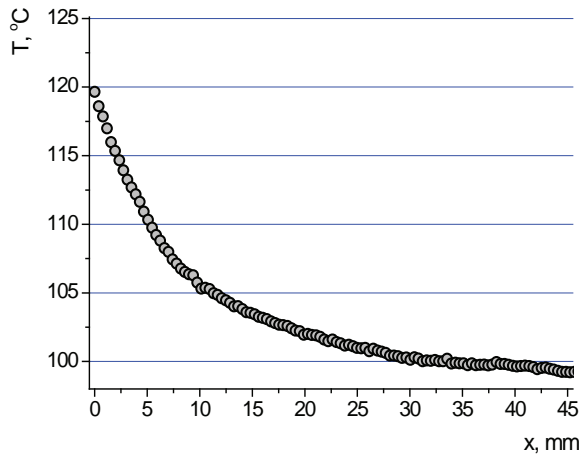


Fig. 2. Temperature distribution along the fin

Visualisation studies conducted from the liquid side of the fin (Fig. 3) reveal that there are two modes of heat transfer present on the fin. At first nucleate boiling regime is observed, which is a highly efficient way of dissipating heat. Here, bubbles and vapour columns are formed as seen in the picture (Fig. 3).

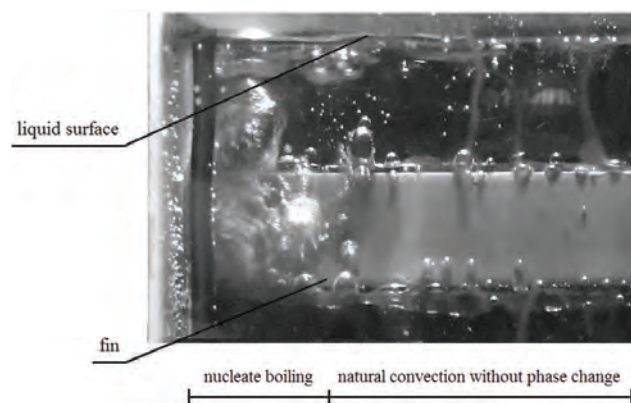


Fig. 3. Heat transfer modes on the fin

Then, heat is transferred through natural convection without phase change. A few bubbles are observed only on the edge of the sample and a sealing. Comparison

on the temperature distribution for the smooth copper fin and the visualisation studies of the boiling modes leads to a conclusion that a change from nucleate boiling into natural convection occurs at superheats of a few Kelvin, which is in agreement with the literature data mentioned earlier [2], so water in the presented experiment is still slightly superheated in the area of the fin where heat is dissipated by natural convection (and just behind the boiling area).

3. Comparison of the experimental results with the model

The method described above enables to determine the relationship for the heat transfer coefficient and, consequently, for heat flux (based on the Newton law). The obtained results will be compared with literature data.

One of the models of boiling heat transfer is based on the assumption of forced convection, which has been applied by Forster and Zuber [3]. They used their own equations for vapour bubble growth and determined that the Reynolds number does not depend on the bubble radius. The equation for heat flux is:

$$q = 0.00122 \left(\frac{\lambda_l^{0.79} c_{pl}^{0.45} \rho_l^{0.49}}{\sigma^{0.5} \mu_l^{0.29} r^{0.24} \rho_v^{0.24}} \right) \theta^{1.24} \Delta P_{sat} \quad (5)$$

where indices l , v , w , sat stand for liquid, vapour, wall and saturation, respectively, while μ is dynamic viscosity, ρ – density, σ – surface tension, r – latent heat of vaporisation, c_p – specific heat and ΔP – difference in saturation pressure corresponding to a difference in saturation temperature equal to the superheat.

Another model was proposed by Rohsenow [6]. Here, heat transfer is affected by the movement of vapour bubbles in the vessel. It is related to the suction of liquid behind bubbles and the creation of convective currents. Consequently, the phenomenon can be modelled as a single phase forced convection. Heat flux can be calculated from the following formula:

$$q = \left(\frac{c_{pl} \theta}{Cr} \right)^{\frac{1}{0.33}} \sqrt{\frac{g(\rho_l - \rho_v)}{\sigma}} \mu_l r \text{Pr}_l^{-\frac{s}{0.33}} \quad (6)$$

Where the values of constants C and s differ depending on the surface morphology, its material and the kind of the boiling liquid, while Pr is the Prandtl number.

The comparison of the experimental and calculation results based on the Rohsenow model are presented in Figure 4. A good congruence is observed in the analysed superheat range.

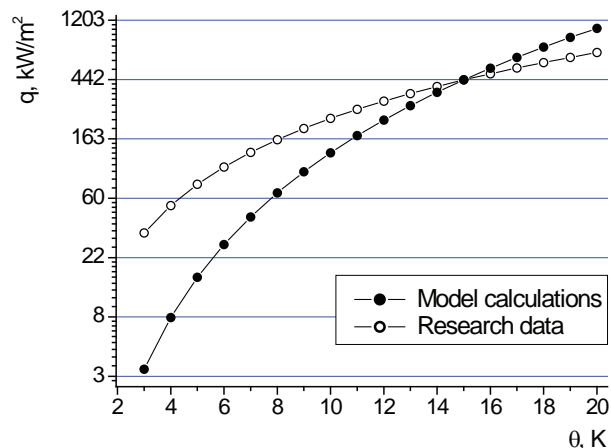


Fig. 4. Boiling curves for the investigated smooth surface and Rohsenow model calculations

4. Conclusions

Boiling heat transfer can be investigated using both temperature measurements e.g. with a thermovision camera, or visualisation studies. Each approach gives an insight into the physics of this phenomenon and enables to better understand the operation of phase change heat exchangers. It can also improve the design of such devices.

References

- [1] Carey V.P.: *Liquid-vapor phase-change phenomena*. An introduction to the thermophysics of vaporization and condensation in heat transfer equipment, Hemisphere, 1992.
- [2] Cengel Y.A.: *Heat Transfer: a practical approach*, McGraw-Hill, 2003.
- [3] Forster, H.M., Zuber N.: *Dynamics of vapor bubbles and boiling heat transfer*, AIChE J., Vol. 1, 1955, pp. 531-535.
- [4] Orman Ł.J.: *Nucleate boiling heat transfer on a smooth surface of a fin*, Proc. of Int. Conf Heat Transfer and Renewable Sources of Energy, 2008, pp. 363-369.
- [5] Orzechowski T.: *Wymiana ciepła przy wrzepieniu na żebach z mikropowierzchnią strukturalną*, Wydawnictwo Politechniki Świętokrzyskiej, Kielce, 2003.
- [6] Rohsenow W.M.: *A method of correlating heat transfer data for surface boiling of liquids*, Trans. ASME, vol. 74, 1952, pp. 969-975.
- [7] Ünal H.C.: *Determination of the temperature distribution in an extended surface with non-uniform heat transfer coefficient*, Int J Heat Mass Transfer, vol. 28, 1985, pp. 2279-2283.

Badania wymiany ciepła przy wrzeniu na pojedynczym żebrze

1. Wprowadzenie

Wymiana ciepła przy wrzeniu umożliwia odprowadzanie znaczących gęstości strumienia ciepła. W związku z tym proces ten jest bardzo interesujący z punktu widzenia poszukiwania nowych możliwości odprowadzania dużych ilości ciepła z urządzeń elektronicznych czy mechanicznych. Możliwe jest również wytwarzanie mniejszych i bardziej efektywnych wymienników ciepła dla przemysłu chłodniczego, jeśli wrzenie będzie odbywać się na specjalnie zaprojektowanych powierzchniach.

Badania wymiany ciepła są zwykle prowadzone na powierzchniach izotermicznych. Niewiele prac dotyczy powierzchni nieizotermicznych, które w praktyce spotykane są najczęściej. W związku z tym należy prowadzić badania właśnie na takich powierzchniach żeber, celem poszerzenia wiedzy na temat analizowanego zjawiska.

Wrzenie rozpoczyna się, gdy temperatura powierzchni zanurzonej w cieczy będzie wyższa niż temperatura nasycenia tej cieczy. Na początku nie pojawiają się pęcherze, a wymiana ciepła odbywa się w drodze konwekcji swobodnej. Później, gdy ciecz jest nieznacznie przegrzana (dla wody wymagane przegrzanie to ok. 2 do 6°C [2]) następuje tworzenie pęcherzy parowych na powierzchni. Jest to wrzenie pęcherzykowe. W tym obszarze wymiana ciepła jest intensywna, a wraz ze wzrostem dostarczanego strumienia ciepła rośnie ilość wytwarzanej pary. Sąsiednie pęcherze łączą się, aż wreszcie na powierzchni wytwarza się film parowy izolujący ją od cieczy. Wówczas gęstość odbieranego strumienia ciepła obniża się. Jest to wrzenie błonowe. Dalszy wzrost gęstości strumienia ciepła odprowadzanego z powierzchni jest związany z radiacyjną wymianą ciepła [1]. Z praktycznego punktu widzenia największe znaczenie ma wrzenie pęcherzykowe.

2. Procedura eksperymentalna i wyniki badań

Przez wiele lat badania wymiany ciepła prowadzono na stanowiskach, w których grzejnik elektryczny regulował temperaturę powierzchni celem wyznaczenia kolejnych punków na krzywej wrzenia, czyli zależności gęstości strumienia ciepła lub współczynnika przejmowania ciepła od temperatury.

Zaprezentowana technika w niniejszym artykule pochodzi z pracy [5]. Podstawowym elementem jest żebro (rys. 1). Stanowi ono część ścianki bocznej naczynia z wrzącą ciecą. Żebro z jednej strony jest w kontakcie z cieczą, a z drugiej z powietrzem i ta strona jest obserwowana kamerą termowizyjną. Ciepło dostarcza się do podstawy żebra. W konsekwencji tworzy się gradient temperatury na długości. W oparciu o zmierzony kamerą termowizyjną rozkład temperatury wyznacza się lokalne wartości współczynnika przejmowania ciepła według metodyki zaprezentowanej przez Orzechowskiego [5].

Rysunek 2 przedstawia rozkład temperatury na powierzchni gładkiego żebra. Łatwo można zauważać, że wrzenie jest bardzo efektywne do chłodzenia rozpatrywanego elementu. Temperatura spada blisko podstawy i osiąga temperaturę nasycenia.

Badania wizualizacyjne wykonane od strony cieczy (rys. 3) ujawniają istnienie dwóch rodzajów wymiany ciepła na żebrze: wrzenia pęcherzykowego przy podstawie z widocznymi pęcherzami parowymi, a dalej konwekcji swobodnej.

3. Porównanie wyników z modelem

W oparciu o przedstawioną metodę można wyznać lokalne wartości współczynnika przejmowania ciepła i porównanie otrzymanych wyników z danymi literaturowymi. Jednym z modeli, opartym o założenie konwekcyjnej wymiany ciepła (konwekcja wymuszona) jest zależność zaproponowana przez Fostera i Zubera [3]. Można również skorzystać

z modelu Rohsenowa [6], w którym zakłada się, że na wymianę ciepła wpływa ruch pęcherzy w cieczy. Porównanie wyników badań z obliczeniami modelowymi prezentuje rysunek 4, na którym można zaobserwować zgodność obydwu wielkości.

4. Wnioski

Wymiana ciepła przy wrzeniu może być analizowana w oparciu o rozkład temperatury na rozpatrywanym elemencie czy badaniach wizualizacyjnych. Obydwie metody dają pogląd na zachodzące procesy i umożliwiają ich lepsze zrozumienie. W oparciu o wyniki takich badań możliwe jest lepsze projektowanie wymienników ciepła, działających w oparciu o zmianę fazy czynnika.

Maria Nowak (Font size 10 pt Times New Roman)
Kielce University of Technology
e-mail: mmmm@tu.kielce.pl

HOW TO PREPARE THE MANUSCRIPT (Font size 14 pt Times New Roman)

Abstract

*The abstract should not exceed 10 lines. It should provide information about the objectives of the work, methods used and test results obtained in the course of the experiments/analyses.
(Font size 10 pt Times New Roman Italic)*

Keywords: phrases, words (Font size 10 pt Times New Roman)

1. Introduction

The introduction should present the background of the work (font size 11 pt Times New Roman).

2. Main text

2.1. General information

The paper volume should not exceed 8 pages of A4 size with font size of 11 pt (Times New Roman). The number in square brackets [1] should be used for quotations. The paper should be sent by email to sae@tu.kielce.pl. The papers in the journal are reviewed.

2.2. Figures

Figures (in black and white or colour) should be of good quality and numbered with the sequence of their appearance in the text. They should be centered and have a caption of 10 pt size. High resolution files *.JPG, *.WMF, *.CDR, *.TIFF, *.EPS, *.BMP files should be used and inserted into the text as well as sent as separate files. 10 pt spacing should be left between the figure and the text.

2.3. Tables

Tables should be centered. Titles should be placed above the tables and written with font size of 10 pt (Times New Roman). The same applies to the text in the table (see example below).

Table 1. Title of the table.

No	table	table	table
1	table	table	table
2	table	table	table
3	table	table	table

2.4. Equations

Equations and formulas should be centered and numbered in brackets. 11 pt spacing should be left between the equation and the text above and below it.

3. Conclusions

References (arranged in the citing order):

- [1] Nowak M.: *Modelowanie konstrukcyjne (Structural modelling)*. Postępy Technologiczne 10 (2000), pp. 30-34.
- [2] Zarylski R.: *Pomiary dynamiczne (Dynamic measurements)*. WNT, Warszawa 1971.

(Font size 10 pt Times New Roman)

Maria Nowak

Tytuł w języku polskim

1. Wprowadzenie

2. Tekst artykułu

Tekst w języku polskim ma odpowiadać swoim układem wersji angielskiej, może być skrócony. Nie powinien zawierać tabel, rysunków, wzorów, a jedynie odniesienie do tych, które znajdują się w wersji angielskiej. Objętość artykułu nie powinna przekraczać 8 stron czcionką 11 (Times New Roman). Bibliografię należy umieszczać w nawiasie kwadratowym [1] i numerować w kolejności alfabetycznej. Artykuły należy przesyłać na adres sae@tu.kielce.pl. Artykuły są recenzowane.

3. Wnioski

THE REVIEW PROCESS

The following requirements need to be met by the paper:

- the title should reflect the content of the paper
- the content should be within the thematic scope of the journal
- the paper should be properly and clearly divided into paragraphs
- original elements need to be part of the paper
- the research method should be properly selected
- adequate references need to be cited
- interpretation and conclusions should match the presented test results
- the paper should not contain parts indicating commercial use

The reviewers:

A. Bartosik, R. Chatys, R. Dachowski, O. Moroz, H. Nowak, L. Lichołaj,
Z. Rymarczyk, V. Sidorov, Z. Tartachynska, A. Zwierzchowska

